A Convex Analysis-Based Minimum-Volume Enclosing Simplex Algorithm for Hyperspectral Unmixing

Tsung-Han Chan, *Student Member, IEEE*, Chong-Yung Chi, *Senior Member, IEEE*, Yu-Min Huang, and Wing-Kin Ma, *Member, IEEE*

***Abstract*—Hyperspectral unmixing aims at identifying the hidden spectral signatures (or endmembers) and their corresponding proportions (or abundances) from an observed hyperspectral scene. Many existing hyperspectral unmixing algorithms were developed under a commonly used assumption that pure pixels exist. However, the pure-pixel assumption may be seriously violated for highly mixed data. Based on intuitive grounds, Craig reported an unmixing criterion without requiring the pure-pixel assumption, which estimates the endmembers by vertices of a minimum-volume simplex enclosing all the observed pixels. In this paper, we incorporate convex analysis and Craig's criterion to develop a minimum-volume enclosing simplex (MVES) formulation for hyperspectral unmixing. A cyclic minimization algorithm for approximating the MVES problem is developed using linear programs (LPs), which can be practically implemented by readily available LP solvers. We also provide a non-heuristic guarantee of our MVES problem formulation, where the existence of pure pixels is proved to be a sufficient condition for MVES to perfectly identify the true endmembers. Some Monte Carlo simulations and real data experiments are presented to demonstrate the efficacy of the proposed MVES algorithm over several existing hyperspectral unmixing methods.**

***Index Terms*—Convex analysis, convex optimization, hyperspectral unmixing, linear programming, minimum-volume enclosing simplex.**

I. Introduction

HYPERSPECTRAL remote sensing [1], [2] is a crucial technique for the identification of disparate material substances from observed spectra, and has been utilized for planetary exploration [3], [4] to analyze the composition and mineralogy of an observed planet in the solar system, e.g., Mars. Hyperspectral imaging also has a wide range of applications to the Earth, such as terrain classification, agricultural monitoring, environmental monitoring, and military surveillance [5]–[8]. When the hyperspectral scene is over solid surfaces, each pixel of the observed spectra usually comprises multiple spectral signatures (or endmembers) due to low spatial resolution of the sensor used. *Hyperspectral unmixing* [9]–[26], a procedure of decomposing the measured spectrum of an observed scene into a collection of endmembers and their corresponding proportions (or abundances), is essential in identifying individual materials from a hyperspectral scene.

In hyperspectral unmixing, basically there are three major processes, namely dimension reduction, endmember extraction, and the inversion process. Dimension reduction is useful for complexity reduction of the subsequent endmember extraction and inversion process. Principal component analysis (PCA) [10] and maximum noise fraction (MNF) [11] are typical dimension reduction algorithms. However, accurate estimation of the number of dimensions that can truly represent the data space still remains a challenging task, for which some model order estimation methods have been developed, for instance, virtual dimensionality (VD) [12] and hyperspectral signal subspace identification by minimum error (HySime) [13]. Endmember extraction is to determine the endmembers that contribute to the measured spectra. A number of endmember extraction algorithms have been reported, e.g., pixel purity index (PPI) [14], N-finder (N-FINDR) [15], [16], vertex component analysis (VCA) [17], and convex cone analysis (CCA) [18]. Finally, the inversion process is to estimate the abundances associated with the endmember estimates. For instance, fully constrained least squares (FCLS) [19] is an effective algorithm for estimating the abundances. Moreover, there are unmixing methods that are capable of determining endmembers and abundances simultaneously, such as alternating projected subgradients (APS) [20], iterated constrained endmembers (ICE) [21], nonnegative matrix factorization (NMF) [22], [23], joint Bayesian approach (JBA) [24], and minimum volume transform (MVT) [25].

A number of endmember extraction algorithms, such as PPI, N-FINDR and VCA, adopt the assumption of existence of pure pixels (i.e., pixels that are fully contributed by a single endmember) in the observed data set. Simply speaking, those algorithms attempt to search for the purest observed pixels over the data set as the endmember estimates, and are usually followed by FCLS to complete hyperspectral unmixing. PPI [14] projects all the observed pixels onto randomly generated unit-norm vectors and counts the number of times (i.e., scores) of

Manuscript received November 17, 2008; accepted May 16, 2009. First published June 19, 2009; current version published October 14, 2009. The associate editor coordinating the review of this manuscript and approving it for publication was Dr. Kainam Thomas Wong. This work was presented at the International Conference of Acoustics, Speech and Signal Processing (ICASSP), Taipei, Taiwan, April 19-24, 2009. This work was supported by the National Science Council (R.O.C.) under Grants NSC 96-2628-E-007-003-MY3 and NSC 96-2628-E-007-002-MY2, and by a grant from the Research Grant Council of Hong Kong (General Research Fund, Project 2150599).

T.-H. Chan, C.-Y. Chi, Y.-M. Huang are with the Institute of Communications Engineering, National Tsing Hua University, Hsinchu, Taiwan, R.O.C. (e-mail: d935608@oz.nthu.edu.tw; cychi@ee.nthu.edu.tw; g9564504@oz.nthu.edu.tw).

W.-K. Ma is with the Department of Electronic Engineering, The Chinese University of Hong Kong, Shatin, N.T., Hong Kong (e-mail: wkma@ieee.org).

Color versions of one or more of the figures in this paper are available online at http://ieeexplore.ieee.org.

Digital Object Identifier 10.1109/TSP.2009.2025802

1053-587X/$26.00 © 2009 IEEE

Authorized licensed use limited to: Chinese University of Hong Kong. Downloaded on October 21, 2009 at 21:45 from IEEE Xplore. Restrictions apply.

the event that the value of each projected pixel reaches an extreme value (either minimum or maximum projected value). Then the purest pixels are identified as those pixels with the highest scores. N-FINDR [15] is based on a criterion that the volume of a simplex formed by the purest pixels is maximum, and fulfills this criterion by inflating the simplex inside the data set. VCA [17] iteratively projects the data onto a vector orthogonal to the subspace spanned by all the obtained endmember estimates before the current iteration, and identifies a new endmember as the one with the extreme value of the projected data. However, for the case of highly mixed data, the pure-pixel assumption may be seriously violated.

Hyperspectral unmixing algorithms that do not require the pure-pixel assumption would be appropriate for highly mixed data. Examples of such algorithms are CCA, APS, ICE, NMF, JBA, and MVT. CCA [18] determines the endmembers by searching for the boundary points of a convex cone constructed from the observed spectra. APS [20] is an alternating projected subgradient approach to solving a least squares problem, through the use of a regularization parameter that controls the difference between each target pixel of the abundances and its neighbors. ICE [21] uses quadratic programming to solve a least squares problem with a regularized term added to the objective function to limit the sum of the variances of the simplex vertices. NMF [22] was originally proposed for object recognition and has been recently applied to hyperspectral unmixing [23]. It decomposes the observation matrix into a product of two nonnegative matrices, one serving as the endmember estimates while the other serving as the abundance estimates. However, NMF may suffer from a nonunique decomposition problem. To provide a more reliable decomposition in hyperspectral unmixing, a variant of NMF, called minimum volume constrained NMF (MVC-NMF) [26], has been proposed. JBA [24] estimates the endmembers by generating the posterior distribution of abundances and endmember parameters under a hierarchical Baysian model that assumes conjugate prior distributions for these parameters. Moreover, Craig [25] reported an unmixing criterion based on the belief that the vertices of a minimum-volume simplex enclosing all the observed pixels should serve as high-fidelity estimates of the endmembers. To find such a simplex, Craig suggested a method (i.e., MVT) that begins with a simplex of large volume and then literally moves the faces of the simplex in toward the data cloud. However, MVT may be computationally intractable when dealing with a large amount of observed pixels.

In this paper, we use convex analysis and optimization to develop a hyperspectral unmixing algorithm, called the minimum-volume enclosing simplex (MVES) algorithm. The endeavor of employing convex analysis is motivated by the fact that some concepts, such as affine hull and convex hull, are quite suitable for analysis of the hyperspectral unmixing problem [27], [28]. We first perform dimension reduction of the observed pixels through a convex analysis concept called affine set fitting [29]. Then we employ Craig's unmixing criterion [25] to formulate the hyperspectral unmixing as an MVES optimization problem. We prove a non-heuristic guarantee of MVES, where we show that the MVES problem leads to unique identification of the true endmembers when pure pixels exist. Thus, MVES is expected to provide unmixing performance at least no worse than other pure-pixel based algorithms. In our formulation, we show how the MVES problem can be properly recast to a form where the MVES feasible set becomes polyhedral (and convex). The MVES objective function is nonconvex, but the MVES problem can be handled in a cyclic fashion by solving a sequence of linear programs (LPs), which can be readily implemented by any available LP solver. Using both simulated and real data, we found numerically that the MVES algorithm is superior in performance over some existing benchmark methods.

We should mention a concurrent development by Li and Bioucas-Dias described in a recent conference paper [30], called minimum volume simplex analysis (MVSA). In that work Craig's criterion is also considered, and unlike this paper the authors used sequential quadratic programming to handle the nonconvex unmixing problem. This very recently emerged method will also be included in our simulation comparison. Simply speaking, we found that MVSA and MVES algorithm are both competitive in performance, and that the MVES algorithm proposed here may slightly outperform the MVSA in most white noise cases with lower purity levels and various signal-to-noise ratios (SNRs).

The organization of this paper is as follows. In Section II, we present the problem statement and some general assumptions in hyperspectral imaging. Section III introduces some concepts of convex analysis for ease of mathematical derivations that follow. Section IV presents the proposed MVES algorithm. Section V presents some simulation results to demonstrate the efficacy of the proposed MVES algorithm. In Section VI, some real data experiments of hyperspectral imaging are presented to evaluate the effectiveness of the proposed MVES algorithm. Finally, some conclusions are drawn in Section VII.

Prior to the ensuing presentation, let us define the following notations for ease of later use:

$\mathbb{R}, \mathbb{R}^N, \mathbb{R}^{M\times N}$	Set of real numbers, N-vectors, $M \times N$ matrices
$\mathbb{R}_+, \mathbb{R}_+^N, \mathbb{R}_+^{M\times N}$	Set of nonnegative real numbers, N-vectors, $M \times N$ matrices
$\mathbf{X}^\dagger$	Moore-Penrose inverse or pseudoinverse of matrix $\mathbf{X}$
$\mathbf{1}_N$	N-vector with all the components equal to unity
$\mathbf{e}_i$	Unit vector of proper dimension with the ith entry equal to unity
$\mathbf{I}_N$	$N \times N$ identity matrix
$\succeq$	Componentwise inequality
$\|\cdot\|$	Euclidean norm
$\det(\mathbf{X})$	Determinant of square matrix $\mathbf{X}$

II. Problem Statement and Assumptions

Consider a scenario where a hyperspectral sensor explores a scene of interest where N distinct yet unknown substances are involved over M spectral bands. The sensor measures solar electromagnetic radiation reflecting from the substances, and further forms a spectral image cube in which each pixel vector

Authorized licensed use limited to: Chinese University of Hong Kong. Downloaded on October 21, 2009 at 21:45 from IEEE Xplore. Restrictions apply.

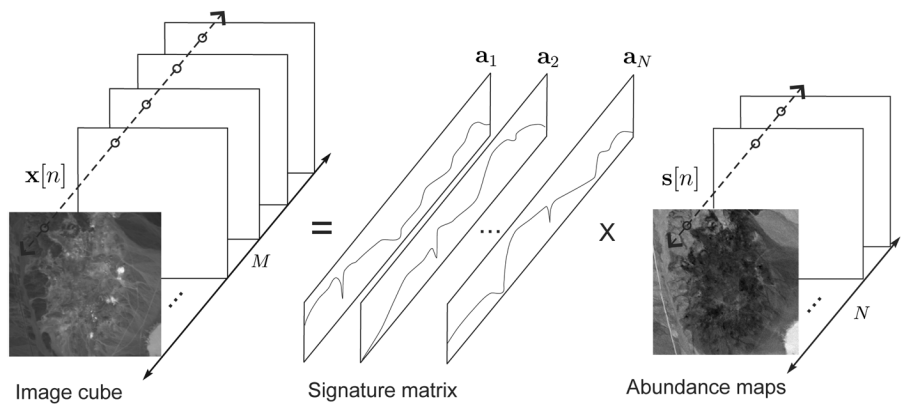

Fig. 1. An illustration of the linear mixing model for hyperspectral imaging.

can be described by the following $M \times N$ linear spectral mixing model:

$$\mathbf{x}[n] = \mathbf{A}\mathbf{s}[n] = \sum_{i=1}^{N} s_i[n]\mathbf{a}_i, \quad n = 1, \ldots, L \tag{1}$$

where $\mathbf{x}[n] = [x_1[n], \ldots, x_M[n]]^T$ is the nth observed pixel vector comprising M spectral bands, $\mathbf{A} = [\mathbf{a}_1, \ldots, \mathbf{a}_N] \in \mathbb{R}^{M \times N}$ denotes the signature matrix whose ith column vector $\mathbf{a}_i$ is the ith endmember signature, $\mathbf{s}[n] = [s_1[n], \ldots, s_N[n]]^T \in \mathbb{R}^N$ is an abundance vector comprising N fractional abundances, and L is the total number of observed pixel vectors. Fig. 1 illustrates the linear spectral mixing model for hyperspectral imaging, where each observed pixel $\mathbf{x}[n]$ is a linear combination of endmember signatures $\mathbf{a}_1, \ldots, \mathbf{a}_N$ weighted by their abundance fractions $s_1[n], \ldots, s_N[n]$.

The goal of hyperspectral unmixing is to estimate the signature matrix $\mathbf{A}$ and the abundances $\mathbf{s}[1], \ldots, \mathbf{s}[L]$ from the observed pixels $\mathbf{x}[1], \ldots, \mathbf{x}[L]$ without prior knowledge about $\mathbf{A}$, $\mathbf{s}[n]$, and the number of endmembers N. Such a problem statement has a lot in common with that of blind source separation (BSS) [31]. However, the interdependence and nonstationarity nature of the abundance maps (or sources) may lead to some difficulty in direct utilization of statistical BSS approaches, such as independent component analysis (ICA) [32], [33].

Like many existing unmixing methods in hyperspectral imaging [5]–[8], the MVES algorithm assumes the number of endmembers N to be known *a priori*. This can be done beforehand by applying model order estimation methods, such as VD [12] and HySime [13]. Furthermore, our MVES algorithm for hyperspectral unmixing is based on the following general assumptions:

A1) (Nonnegativity condition) For all $i = 1, \ldots, N$ and $n = 1, \ldots, L$, $s_i[n] \geq 0$.

A2) (Full additivity condition) For all $n = 1, \ldots, L$, $\sum_{i=1}^{N} s_i[n] = 1$.

A3) $\min\{L, M\} \geq N$ and $\mathbf{A}$ is of full column rank.

Assumption A1) is true in hyperspectral imaging because intensities of all the abundance vectors must be nonnegative. Assumption A2) holds true because the fractional abundances are the proportion distribution of all the endmembers in every observed pixel. Assumption A3) is generally valid because the hyperspectral scene of interest [1], [2], [5]–[8] often involves a large number of image pixels and spectral bands but only a small number of endmembers.

III. Some Basic Concepts of Convex Analysis

This work will extensively use two convex analysis concepts, namely affine hull and convex hull [34]. A concise review of these two concepts and some essential properties is presented in this section.

A. Affine Hull

Given a set of vectors $\{\mathbf{a}_1, \ldots, \mathbf{a}_N\} \subset \mathbb{R}^M$, the *affine hull* of $\{\mathbf{a}_1, \ldots, \mathbf{a}_N\}$ is defined as

$$\mathrm{aff}\{\mathbf{a}_1, \ldots, \mathbf{a}_N\} = \left\{ \mathbf{x} = \sum_{i=1}^{N} \theta_i \mathbf{a}_i \middle| \boldsymbol{\theta} \in \mathbb{R}^N, \mathbf{1}_N^T \boldsymbol{\theta} = 1 \right\} \tag{2}$$

where $\boldsymbol{\theta} = [\theta_1, \ldots, \theta_N]^T$. An affine hull is an affine set, and, therefore, can always be represented as

$$\mathrm{aff}\{\mathbf{a}_1, \ldots, \mathbf{a}_N\} = \left\{ \mathbf{x} = \mathbf{C}\boldsymbol{\alpha} + \mathbf{d} \middle| \boldsymbol{\alpha} \in \mathbb{R}^P \right\} \triangleq \mathcal{A}(\mathbf{C}, \mathbf{d}) \tag{3}$$

where $\mathcal{A}(\cdot, \cdot)$ denotes an affine set parameterized by a 2-tuple $(\mathbf{C}, \mathbf{d}) \in \mathbb{R}^{M \times P} \times \mathbb{R}^M$, with $\mathrm{rank}(\mathbf{C}) = P$. Here, P is the affine dimension of $\mathrm{aff}\{\mathbf{a}_1, \ldots, \mathbf{a}_N\}$, and must satisfy $P \leq N - 1$. If $\{\mathbf{a}_1, \ldots, \mathbf{a}_N\}$ is affinely independent (which means that $\{\mathbf{a}_1 - \mathbf{a}_N, \ldots, \mathbf{a}_{N-1} - \mathbf{a}_N\}$ is linearly independent), then $P = N - 1$.

An interesting question is how to obtain an affine set parameter $(\mathbf{C}, \mathbf{d})$, given $\{\mathbf{a}_1, \ldots, \mathbf{a}_N\}$ and P. This affine set construction problem is very simple for the special case of $P = N - 1$, where a solution is $\mathbf{C} = [\mathbf{a}_1 - \mathbf{a}_N, \ldots, \mathbf{a}_{N-1} - \mathbf{a}_N] \in \mathbb{R}^{M \times (N-1)}$ and $\mathbf{d} = \mathbf{a}_N$. For the general case of $P < N - 1$, the 2-tuple $(\mathbf{C}, \mathbf{d})$ can be found by solving the following affine set fitting problem [29]:

$$(\mathbf{C}, \mathbf{d}) = \arg \min_{\substack{\mathbf{C}, \mathbf{d} \\ \mathbf{C}^T \mathbf{C} = \mathbf{I}_P}} \sum_{i=1}^{N} e_{\mathcal{A}(\mathbf{C}, \mathbf{d})}(\mathbf{a}_i) \tag{4}$$

where $e_{\mathcal{A}}(\mathbf{a}_i)$ is the projection error of $\mathbf{a}_i$ onto the set $\mathcal{A}$, defined as

$$e_{\mathcal{A}}(\mathbf{a}_i) = \min_{\mathbf{a} \in \mathcal{A}} \|\mathbf{a}_i - \mathbf{a}\|^2 \tag{5}$$

Authorized licensed use limited to: Chinese University of Hong Kong. Downloaded on October 21, 2009 at 21:45 from IEEE Xplore. Restrictions apply.

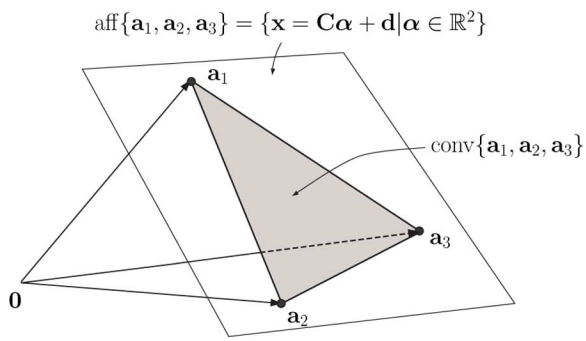

Fig. 2. Geometric illustration of affine hull, convex hull, and vertices for $N = 3$.

and the constraint $\mathbf{C}^T\mathbf{C} = \mathbf{I}_P$ is to restrict $\mathbf{C}$ to have $\mathrm{rank}(\mathbf{C}) = P$. The problem in (4) finds a $(\mathbf{C},\mathbf{d})$ such that $\{\mathbf{a}_1,\ldots,\mathbf{a}_N\}$ has the minimum total projection error with respect to the affine set $\mathcal{A}(\mathbf{C},\mathbf{d})$ (which will be zero in the absence of additive noise). It is shown that problem (4) has a simple closed-form solution [29] given by

$$\mathbf{d} = \frac{1}{N}\sum_{i=1}^{N}\mathbf{a}_i \tag{6}$$

$$\mathbf{C} = \left[\boldsymbol{q}_1(\mathbf{U}\mathbf{U}^T), \boldsymbol{q}_2(\mathbf{U}\mathbf{U}^T), \ldots, \boldsymbol{q}_P(\mathbf{U}\mathbf{U}^T)\right] \tag{7}$$

where $\mathbf{U} = [\mathbf{a}_1 - \mathbf{d}, \ldots, \mathbf{a}_N - \mathbf{d}] \in \mathbb{R}^{M\times N}$, and $\boldsymbol{q}_i(\mathbf{R})$ is the eigenvector associated with the ith principal eigenvalue of the square matrix $\mathbf{R}$. It is worth noticing that if the given $\{\mathbf{a}_1,\ldots,\mathbf{a}_N\}$ is a noisy or corrupted version of their true counterpart, then affine set fitting provides a least-squares estimate of the true affine set for any chosen P.

B. Convex Hull

Given a set of vectors $\{\mathbf{a}_1,\ldots,\mathbf{a}_N\} \subset \mathbb{R}^M$, the *convex hull* of $\{\mathbf{a}_1,\ldots,\mathbf{a}_N\}$ is defined as

$$\mathrm{conv}\{\mathbf{a}_1,\ldots,\mathbf{a}_N\} = \left\{\mathbf{x} = \sum_{i=1}^{N}\theta_i\mathbf{a}_i \middle| \boldsymbol{\theta} \in \mathbb{R}_+^N, \mathbf{1}_N^T\boldsymbol{\theta} = 1\right\}. \tag{8}$$

A convex hull is called a *simplex* if $M = N-1$ and $\mathbf{a}_1,\ldots,\mathbf{a}_N$ are affinely independent. A point $\mathbf{x} \in \mathrm{conv}\{\mathbf{a}_1,\ldots,\mathbf{a}_N\}$ is a *vertex* (or extreme point) of $\mathrm{conv}\{\mathbf{a}_1,\ldots,\mathbf{a}_N\}$ if $\mathbf{x}$ cannot be a nontrivial convex combination of $\mathbf{a}_1,\ldots,\mathbf{a}_N$ (more specifically, $\mathbf{x} \neq \sum_{i=1}^N \theta_i\mathbf{a}_i$ for all $\boldsymbol{\theta} \in \mathbb{R}_+^N$, $\mathbf{1}_N^T\boldsymbol{\theta} = 1$, and $\boldsymbol{\theta} \neq \mathbf{e}_i$ for any i). For a general convex hull, the set of all of its vertices is a subset of $\{\mathbf{a}_1,\ldots,\mathbf{a}_N\}$, but, for a simplex, the set is exactly $\{\mathbf{a}_1,\ldots,\mathbf{a}_N\}$.

A geometric illustration of affine hull, convex hull, and vertices for $N = 3$ is given in Fig. 2. The affine hull of $\{\mathbf{a}_1,\mathbf{a}_2,\mathbf{a}_3\}$ is the hyperplane passing through the three points $\mathbf{a}_1,\mathbf{a}_2,\mathbf{a}_3$, and the convex hull is the triangle on the hyperplane with the three vertices $\mathbf{a}_1,\mathbf{a}_2,\mathbf{a}_3$.

IV. Minimum-Volume Enclosing Simplex Algorithm

Considering the signal model in (1) under the full additivity condition of the abundance vectors [A2)], one can immediately infer that

$$\mathbf{x}[n] \in \mathrm{aff}\{\mathbf{a}_1,\ldots,\mathbf{a}_N\},\ \forall\, n. \tag{9}$$

In addition, we can recover the affine hull of $\mathbf{a}_1,\ldots,\mathbf{a}_N$ from the given observed pixels $\mathbf{x}[1],\mathbf{x}[2],\ldots,\mathbf{x}[L]$. Consider the following lemma.

Lemma 1. (Affine Hull Consistency [29]): Under A2) and A3)

$$\mathrm{aff}\{\mathbf{x}[1],\ldots,\mathbf{x}[L]\} = \mathrm{aff}\{\mathbf{a}_1,\ldots,\mathbf{a}_N\}. \tag{10}$$

Since $\mathbf{a}_1,\ldots,\mathbf{a}_N$ are linearly independent [as assumed in A3)], the endmember affine hull $\mathrm{aff}\{\mathbf{a}_1,\ldots,\mathbf{a}_N\}$ can be represented by

$$\mathrm{aff}\{\mathbf{a}_1,\ldots,\mathbf{a}_N\} = \left\{\mathbf{x} = \mathbf{C}\boldsymbol{\alpha} + \mathbf{d} \middle| \boldsymbol{\alpha} \in \mathbb{R}^{N-1}\right\} \triangleq \mathcal{A}(\mathbf{C},\mathbf{d}) \tag{11}$$

for some $(\mathbf{C},\mathbf{d}) \in \mathbb{R}^{M\times(N-1)} \times \mathbb{R}^M$ and $\mathrm{rank}(\mathbf{C}) = N-1$. From Lemma 1 and (11), the affine hull parameter pair $(\mathbf{C},\mathbf{d})$ for both $\mathrm{aff}\{\mathbf{a}_1,\ldots,\mathbf{a}_N\}$ and $\mathrm{aff}\{\mathbf{x}[1],\ldots,\mathbf{x}[L]\}$ can be estimated through the affine set fitting (as presented in Section III) as follows:

$$\mathbf{d} = \frac{1}{L}\sum_{n=1}^{L}\mathbf{x}[n],\ (\text{by } (6)) \tag{12}$$

$$\mathbf{C} = \left[\boldsymbol{q}_1(\mathbf{U}\mathbf{U}^T), \boldsymbol{q}_2(\mathbf{U}\mathbf{U}^T), \ldots, \boldsymbol{q}_{N-1}(\mathbf{U}\mathbf{U}^T)\right],\ (\text{by } (7)) \tag{13}$$

where $\mathbf{U} = [\mathbf{x}[1] - \mathbf{d}, \ldots, \mathbf{x}[L] - \mathbf{d}] \in \mathbb{R}^{M\times L}$.

Since $\mathbf{x}[n] \in \mathcal{A}(\mathbf{C},\mathbf{d})$, we can write its affine representation as

$$\mathbf{x}[n] = \mathbf{C}\tilde{\mathbf{x}}[n] + \mathbf{d} \tag{14}$$

where $\tilde{\mathbf{x}}[n]$ is the inverse image of $\mathbf{x}[n]$ under (14), i.e.

$$\tilde{\mathbf{x}}[n] = \mathbf{C}^\dagger(\mathbf{x}[n] - \mathbf{d}) \in \mathbb{R}^{N-1}. \tag{15}$$

The affinely transformed data $\tilde{\mathbf{x}}[1],\ldots,\tilde{\mathbf{x}}[L]$ can be thought of as dimension-reduced pixels. It follows by substituting (1) into (15) that

$$\tilde{\mathbf{x}}[n] = \sum_{j=1}^{N} s_j[n]\mathbf{C}^\dagger\mathbf{a}_j - \mathbf{C}^\dagger\mathbf{d}. \tag{16}$$

Since $\sum_{j=1}^N s_j[n] = 1$ [A2)], the dimension-reduced pixels $\tilde{\mathbf{x}}[n]$ can be expressed as

$$\tilde{\mathbf{x}}[n] = \sum_{j=1}^{N} s_j[n](\mathbf{C}^\dagger\mathbf{a}_j - \mathbf{C}^\dagger\mathbf{d}) = \sum_{j=1}^{N} s_j[n]\boldsymbol{\alpha}_j \tag{17}$$

where

$$\boldsymbol{\alpha}_j = \mathbf{C}^\dagger(\mathbf{a}_j - \mathbf{d}) \in \mathbb{R}^{N-1} \tag{18}$$

is the jth dimension-reduced endmember. The formulation given by (17) not only reduces the computational complexity of the subsequent processing steps, but also enables us to apply the simplex geometry concept to the dimension-reduced pixels $\tilde{\mathbf{x}}[1],\ldots,\tilde{\mathbf{x}}[L]$, as stated in the following lemma.

Lemma 2. (Simplex Geometry): Under A1), A2), and A3),

$$\tilde{\mathbf{x}}[n] \in \mathrm{conv}\{\boldsymbol{\alpha}_1,\ldots,\boldsymbol{\alpha}_N\} \subset \mathbb{R}^{N-1},\ \forall\, n \tag{19}$$

and $\mathrm{conv}\{\boldsymbol{\alpha}_1,\ldots,\boldsymbol{\alpha}_N\}$ is a simplex.

Proof: It is easy to see from A1) and (17) that (19) is true. Next, let us prove that $\mathrm{conv}\{\boldsymbol{\alpha}_1,\ldots,\boldsymbol{\alpha}_N\}$ is a simplex.

Authorized licensed use limited to: Chinese University of Hong Kong. Downloaded on October 21, 2009 at 21:45 from IEEE Xplore. Restrictions apply.

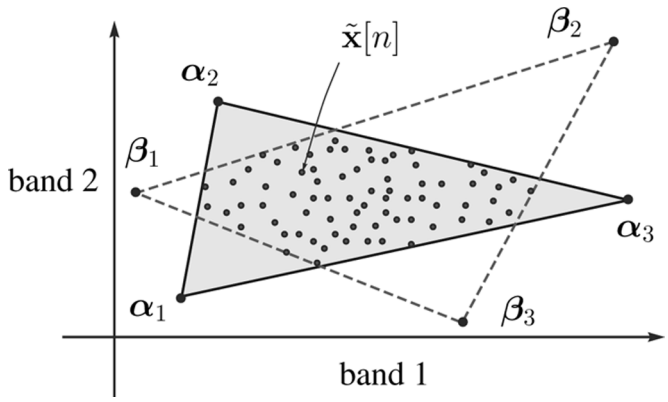

Fig. 3. Scatter plot of two-dimensional dimension-reduced pixels illustrating the MVES problem for hyperspectral unmixing.

Assume that $\{\boldsymbol{\alpha}_1, \ldots, \boldsymbol{\alpha}_N\}$ is affinely dependent, i.e., there exists an $\boldsymbol{\alpha}_j = \sum_{i \neq j}^{N} \theta_i \boldsymbol{\alpha}_i$ where $\sum_{i \neq j}^{N} \theta_i = 1$. One then has $\mathbf{a}_j = \mathbf{C}\boldsymbol{\alpha}_j + \mathbf{d} = \sum_{i \neq j}^{N} \theta_i \mathbf{a}_i$ where $\sum_{i \neq j}^{N} \theta_i = 1$ by (18), implying $\mathbf{a}_1, \ldots, \mathbf{a}_N$ are affinely dependent (or linearly dependent), which is a contradiction to A3). ■

Lemma 2 implies that all the dimension-reduced pixels $\tilde{\mathbf{x}}[1], \ldots, \tilde{\mathbf{x}}[L]$ must be inside the simplex constructed by the dimension-reduced endmembers $\boldsymbol{\alpha}_i$ for $i = 1, \ldots, N$. This key property is geometrically illustrated in Fig. 3. In the figure, we also demonstrate that $\tilde{\mathbf{x}}[1], \ldots, \tilde{\mathbf{x}}[L]$ can also be enclosed by a different simplex, denoted by $\mathrm{conv}\{\boldsymbol{\beta}_1, \ldots, \boldsymbol{\beta}_N\}$. Nevertheless, by intuitive grounds, one would expect that the data enclosing simplex with the minimum volume should coincide with the true endmember simplex $\mathrm{conv}\{\boldsymbol{\alpha}_1, \ldots, \boldsymbol{\alpha}_N\}$. This is exactly the belief of Craig's unmixing criterion [25]. The problem of finding an MVES has been considered in computational geometry [35], [36], where the existing algorithms are combinatorial in nature and could be too complex to practically run for $N > 4$. In what follows, we will consider an optimization formulation for MVES that enables us to utilize LPs to approximate the problem. A sufficient condition for the MVES belief to identify the endmembers will also be proven.

A. MVES Problem for Hyperspectral Unmixing

The problem of finding an MVES can be formulated as an optimization problem as follows:

$$\boxed{\begin{array}{ll} \min\limits_{\boldsymbol{\beta}_1, \ldots, \boldsymbol{\beta}_N} & V(\boldsymbol{\beta}_1, \ldots, \boldsymbol{\beta}_N) \\ \text{s.t.} & \tilde{\mathbf{x}}[n] \in \mathrm{conv}\{\boldsymbol{\beta}_1, \ldots, \boldsymbol{\beta}_N\}, \ \forall\, n \end{array}} \tag{20}$$

where $V(\boldsymbol{\beta}_1, \ldots, \boldsymbol{\beta}_N)$ is the volume of the simplex $\mathrm{conv}\{\boldsymbol{\beta}_1, \ldots, \boldsymbol{\beta}_N\} \subset \mathbb{R}^{N-1}$ given by [37]

$$V(\boldsymbol{\beta}_1, \ldots, \boldsymbol{\beta}_N) = \frac{|\det(\boldsymbol{\Delta}(\boldsymbol{\beta}_1, \ldots, \boldsymbol{\beta}_N))|}{(N-1)!} \tag{21}$$

where

$$\boldsymbol{\Delta}(\boldsymbol{\beta}_1, \ldots, \boldsymbol{\beta}_N) = \begin{bmatrix} \boldsymbol{\beta}_1 & \ldots & \boldsymbol{\beta}_N \\ 1 & \ldots & 1 \end{bmatrix}. \tag{22}$$

Let us consider the endmember identifiability of the MVES criterion, that is, a condition under which the optimal solution of (20) is identical to $\{\boldsymbol{\alpha}_1, \ldots, \boldsymbol{\alpha}_N\}$. Consider the following assumption

A4) (Pure pixel assumption) There exists at least one index set $\{\ell_1, \ell_2, \ldots, \ell_N\}$ such that $\tilde{\mathbf{x}}[\ell_i] = \boldsymbol{\alpha}_i$ for $i = 1, \ldots, N$.

The above assumption is frequently employed in pure-pixel based hyperspectral unmixing methods [14], [15], [17], and may be valid for certain hyperspectral scenes. Also, note that A4) never assumes prior knowledge of the pure pixel positions in the dimension reduced data; that is, $\{\ell_1, \ell_2, \ldots, \ell_N\}$. We have the following theorem.

Theorem 1. (Endmember Identifiability): Under A4), the optimal solution of (20) is uniquely given by $\boldsymbol{\alpha}_1, \ldots, \boldsymbol{\alpha}_N$.

Proof: The constraint of (20) can be equivalently written as

$$\mathrm{conv}\{\tilde{\mathbf{x}}[1], \ldots, \tilde{\mathbf{x}}[L]\} \subseteq \mathrm{conv}\{\boldsymbol{\beta}_1, \ldots, \boldsymbol{\beta}_N\}. \tag{23}$$

Under A4), we can have

$$\begin{aligned} \mathrm{conv}\{\tilde{\mathbf{x}}[1], \ldots, \tilde{\mathbf{x}}[L]\} &= \mathrm{conv}\{\tilde{\mathbf{x}}[\ell_1], \ldots, \tilde{\mathbf{x}}[\ell_N]\} \\ &= \mathrm{conv}\{\boldsymbol{\alpha}_1, \ldots, \boldsymbol{\alpha}_N\}. \end{aligned} \tag{24}$$

Hence, (23) becomes $\mathrm{conv}\{\boldsymbol{\alpha}_1, \ldots, \boldsymbol{\alpha}_N\} \subseteq \mathrm{conv}\{\boldsymbol{\beta}_1, \ldots, \boldsymbol{\beta}_N\}$, which means $\boldsymbol{\alpha}_i \in \mathrm{conv}\{\boldsymbol{\beta}_1, \ldots, \boldsymbol{\beta}_N\}$, i.e.,

$$\boldsymbol{\alpha}_i = \sum_{j=1}^{N} \theta_{ij} \boldsymbol{\beta}_j \tag{25}$$

where $\sum_{j=1}^{N} \theta_{ij} = 1$ and $\theta_{ij} \geq 0$ for $i = 1, \ldots, N$. Then, from (22) and (25), one can easily infer that

$$\boldsymbol{\Delta}(\boldsymbol{\alpha}_1, \ldots, \boldsymbol{\alpha}_N) = \boldsymbol{\Delta}(\boldsymbol{\beta}_1, \ldots, \boldsymbol{\beta}_N)\boldsymbol{\Theta}^T \tag{26}$$

where $\boldsymbol{\Theta} = [\theta_{ij}] \in \mathbb{R}_+^{N \times N}$ and $\boldsymbol{\Theta}\mathbf{1}_N = \mathbf{1}_N$. By (26) and (21), we can have

$$V(\boldsymbol{\alpha}_1, \ldots, \boldsymbol{\alpha}_N) = \frac{\left|\det\left(\boldsymbol{\Delta}(\boldsymbol{\beta}_1, \ldots, \boldsymbol{\beta}_N)\boldsymbol{\Theta}^T\right)\right|}{(N-1)!} \tag{27}$$

$$= V(\boldsymbol{\beta}_1, \ldots, \boldsymbol{\beta}_N)\,|\det(\boldsymbol{\Theta})|. \tag{28}$$

According to Lemma 1 reported in [38], we have $|\det(\boldsymbol{\Theta})| \leq 1$ and the equality holds if and only if $\boldsymbol{\Theta}$ is a permutation matrix. Hence, we can easily see from (28) that

$$V(\boldsymbol{\alpha}_1, \ldots, \boldsymbol{\alpha}_N) \leq V(\boldsymbol{\beta}_1, \ldots, \boldsymbol{\beta}_N) \tag{29}$$

and that the equality holds (or the optimality of (20) is achieved) if and only if $\boldsymbol{\Theta}$ is a permutation matrix. This further implies that the optimum solution for $\{\boldsymbol{\beta}_1, \ldots, \boldsymbol{\beta}_N\}$ is exactly $\{\boldsymbol{\alpha}_1, \ldots, \boldsymbol{\alpha}_N\}$ by (25). ■

It should be pointed out that Theorem 1 provides a sufficient identifiability condition, but not a necessary one. We found that accurate endmember identification could still be possible in the absence of pure pixels, by our experience. So far our conjecture is that if there exist pixels that are close to pure pixels within

Authorized licensed use limited to: Chinese University of Hong Kong. Downloaded on October 21, 2009 at 21:45 from IEEE Xplore. Restrictions apply.

some amount of tolerance, there is a good chance for MVES to achieve accurate endmember identification.

B. MVES Algorithm

We now describe the optimization algorithm proposed for MVES. An alternative expression of the cost function in (20) is given by [37]

$$V(\boldsymbol{\beta}_1,\ldots,\boldsymbol{\beta}_N)=\frac{|\det(\mathbf{B})|}{(N-1)!} \tag{30}$$

where

$$\mathbf{B}=[\boldsymbol{\beta}_1-\boldsymbol{\beta}_N,\ldots,\boldsymbol{\beta}_{N-1}-\boldsymbol{\beta}_N]\in\mathbb{R}^{(N-1)\times(N-1)}. \tag{31}$$

Moreover, any dimension-reduced pixel $\tilde{\mathbf{x}}[n]\in\operatorname{conv}\{\boldsymbol{\beta}_1,\ldots,\boldsymbol{\beta}_N\}$ can be represented by

$$\tilde{\mathbf{x}}[n]=\sum_{i=1}^{N}s_i[n]\boldsymbol{\beta}_i=\boldsymbol{\beta}_N+\mathbf{B}\mathbf{s}'[n] \tag{32}$$

where $\mathbf{s}'[n]=(s_1[n],\ldots,s_{N-1}[n])^T\succeq\mathbf{0}$ and $s_N[n]=1-\mathbf{1}_{N-1}^T\mathbf{s}'[n]\geq 0$. Therefore, problem (20) is equivalent to

$$\begin{aligned}\min_{\substack{\mathbf{B},\boldsymbol{\beta}_N,\\ \mathbf{s}'[1],\ldots,\mathbf{s}'[L]}}\quad & |\det(\mathbf{B})| && (33a)\\ \text{s.t.}\quad & \mathbf{s}'[n]\succeq\mathbf{0},\mathbf{1}_{N-1}^T\mathbf{s}'[n]\leq 1 && (33b)\\ & \tilde{\mathbf{x}}[n]=\boldsymbol{\beta}_N+\mathbf{B}\mathbf{s}'[n]\qquad\forall\, n=1,\ldots,L. && (33c)\end{aligned}$$

Problem (33) is nonconvex. While the nonconvexity of the objective function $|\det(\mathbf{B})|$ is an obstacle, the nonlinear equality constraints in (33c) impose additional difficulty.

We propose a reformulation of (33) where the original nonconvex constraints are transformed into convex constraints. Consider the following one-to-one mappings of the optimization variables:

$$\mathbf{H}=\mathbf{B}^{-1}\in\mathbb{R}^{(N-1)\times(N-1)} \tag{34a}$$
$$\mathbf{g}=\mathbf{B}^{-1}\boldsymbol{\beta}_N\in\mathbb{R}^{N-1}. \tag{34b}$$

Then $\mathbf{s}'[n]$ can be represented by

$$\mathbf{s}'[n]=\mathbf{B}^{-1}(\tilde{\mathbf{x}}[n]-\boldsymbol{\beta}_N)=\mathbf{H}\tilde{\mathbf{x}}[n]-\mathbf{g}. \tag{35}$$

Substituting (34) and (35) into (33), we obtain an equivalent problem of (33)

$$\boxed{\begin{aligned}\max_{\mathbf{H},\mathbf{g}}\quad & |\det(\mathbf{H})|\\ \text{s.t.}\quad & \mathbf{H}\tilde{\mathbf{x}}[n]-\mathbf{g}\succeq\mathbf{0},\\ & \mathbf{1}_{N-1}^T(\mathbf{H}\tilde{\mathbf{x}}[n]-\mathbf{g})\leq 1,\ \forall\, n=1,\ldots,L.\end{aligned}} \tag{36}$$

in which all constraints are linear (and convex).

The equivalent MVES problem in (36) has a convex feasible set, but its objective is still nonconvex. Nevertheless, the problem structures of (36) provide an opportunity for us to use the efficient LPs to tackle the problem. The idea is motivated by the cofactor expansion for $\det(\mathbf{H})$ as follows:

$$\det(\mathbf{H})=\sum_{j=1}^{N-1}(-1)^{i+j}h_{ij}\det(\boldsymbol{\mathcal{H}}_{ij}) \tag{37}$$

for any $i=1,\ldots,N-1$, where h_{ij} is the (i,j)th entry of $\mathbf{H}$, and $\boldsymbol{\mathcal{H}}_{ij}\in\mathbb{R}^{(N-2)\times(N-2)}$ is a submatrix of $\mathbf{H}$ with the ith row and jth column removed [37]. Note that with a fixed $\boldsymbol{\mathcal{H}}_{ij}$, $\det(\mathbf{H})$ is a linear function of h_{ij}, $j=1,2,\ldots,N-1$. Let us consider updating one row vector of $\mathbf{H}$ and one entry of $\mathbf{g}$ while fixing the other rows of $\mathbf{H}$ and the other entries of $\mathbf{g}$. Let $\mathbf{h}_i^T$ denote the ith row vector of $\mathbf{H}$, and g_i denote the ith entry of $\mathbf{g}$. The partial maximization of (36) with respect to $\mathbf{h}_i$ and g_i is given by

$$\begin{aligned}\max_{\mathbf{h}_i^T,g_i}\quad & \left|\sum_{j=1}^{N-1}(-1)^{i+j}h_{ij}\det(\boldsymbol{\mathcal{H}}_{ij})\right|\\ \text{s.t.}\quad & 0\leq\mathbf{h}_i^T\tilde{\mathbf{x}}[n]-g_i\leq 1-\sum_{j\neq i}(\mathbf{h}_j^T\tilde{\mathbf{x}}[n]-g_j),\quad\forall\, n.\end{aligned} \tag{38}$$

Note that the objective function in (38) is still nonconvex. However, the partial maximization problem in (38) can be solved in a globally optimal manner by breaking it into two LPs

$$\begin{aligned}p^\star=\max_{\mathbf{h}_i^T,g_i}\ & \sum_{j=1}^{N-1}(-1)^{i+j}h_{ij}\det(\boldsymbol{\mathcal{H}}_{ij})\\ \text{s.t. } & 0\leq\mathbf{h}_i^T\tilde{\mathbf{x}}[n]-g_i\leq 1-\sum_{j\neq i}(\mathbf{h}_j^T\tilde{\mathbf{x}}[n]-g_j)\qquad\forall\, n\end{aligned} \tag{39a}$$

$$\begin{aligned}q^\star=\min_{\mathbf{h}_i^T,g_i}\ & \sum_{j=1}^{N-1}(-1)^{i+j}h_{ij}\det(\boldsymbol{\mathcal{H}}_{ij})\\ \text{s.t. } & 0\leq\mathbf{h}_i^T\tilde{\mathbf{x}}[n]-g_i\leq 1-\sum_{j\neq i}(\mathbf{h}_j^T\tilde{\mathbf{x}}[n]-g_j)\qquad\forall\, n.\end{aligned} \tag{39b}$$

The optimal solution of (38), denoted by $((\mathbf{h}_i^T)^\star, g_i^\star)$, is chosen as the optimal solution of (39a) if $|p^\star|>|q^\star|$, and the optimal solution of (39b) if $|q^\star|>|p^\star|$. This row-wise minimization is conducted cyclically (i.e., $i:=(i\operatorname{modulo}(N-1))+1$ at each iteration) until some stopping rule is satisfied.

Suppose that a solution $(\mathbf{H}^\star,\mathbf{g}^\star)$ is obtained by cyclic maximization of (36). By (31) and (34) the dimension-reduced endmember estimates, denoted by $\widehat{\boldsymbol{\alpha}}_1,\ldots,\widehat{\boldsymbol{\alpha}}_N$, are obtained by

$$\widehat{\boldsymbol{\alpha}}_N=(\mathbf{H}^\star)^{-1}\mathbf{g}^\star \tag{40}$$
$$[\widehat{\boldsymbol{\alpha}}_1,\ldots,\widehat{\boldsymbol{\alpha}}_{N-1}]=\widehat{\boldsymbol{\alpha}}_N\mathbf{1}_{N-1}^T+(\mathbf{H}^\star)^{-1}. \tag{41}$$

Authorized licensed use limited to: Chinese University of Hong Kong. Downloaded on October 21, 2009 at 21:45 from IEEE Xplore. Restrictions apply.

The endmember signatures can then be recovered by (18), i.e., $\widehat{\mathbf{a}}_i = \mathbf{C}\widehat{\boldsymbol{\alpha}}_i + \mathbf{d}$ for $i = 1, \ldots, N$. Furthermore, from (35), the abundance vectors can be estimated as

$$\begin{aligned}\widehat{\mathbf{s}}[n] &= [\mathbf{s}'[n]^T \quad 1 - \mathbf{1}_{N-1}^T \mathbf{s}'[n]]^T \\ &= \left[(\mathbf{H}^\star \tilde{\mathbf{x}}[n] - \mathbf{g}^\star)^T \quad 1 - \mathbf{1}_{N-1}^T (\mathbf{H}^\star \tilde{\mathbf{x}}[n] - \mathbf{g}^\star)\right]^T \quad \forall\, n.\end{aligned} \tag{42}$$

Therefore, the proposed MVES algorithm yields the estimates of the endmembers and abundances given by (40), (41), and (42) simultaneously without involving any inversion process.

To initialize the proposed MVES algorithm, a feasible $(\mathbf{H}, \mathbf{g})$ for problem (38) is needed. We can find one feasible $(\mathbf{H}, \mathbf{g})$ by solving the following feasibility problem:

$$\begin{aligned} \text{find} \quad & (\mathbf{H}, \mathbf{g}) \\ \text{s.t.} \quad & \mathbf{H}\tilde{\mathbf{x}}[n] - \mathbf{g} \succeq \mathbf{0} \\ & \mathbf{1}_{N-1}^T (\mathbf{H}\tilde{\mathbf{x}}[n] - \mathbf{g}) \le 1, \quad \forall n = 1, \ldots, L \end{aligned} \tag{43}$$

which can also be implemented by LP.

The proposed MVES algorithm is summarized in Table I. If the LP solver used is a primal-dual interior-point method [39], [40], then each LP problem in (39a) or (39b) can be solved practically with a worst-case computational complexity of $\mathcal{O}(L^{0.5}(2LN + N^3)) \simeq \mathcal{O}(NL^{1.5})$ for $L \gg N$ [29]. Moreover, the proposed MVES algorithm involves $2N$ LPs per iteration, implying that its worst-case computational complexity order is $\mathcal{O}(N^2 L^{1.5})$ per iteration.

TABLE I
THE PROPOSED MVES ALGORITHM FOR HYPERSPECTRAL UNMIXING

Given A convergence tolerance $\varepsilon > 0$, the observed pixels $\mathbf{x}[n]$ for $n = 1, \ldots, L$, and the number of endmembers N.

Step 1. Find the endmember affine set parameters $(\mathbf{C}, \mathbf{d})$ by

$$\mathbf{d} = \frac{1}{L}\sum_{n=1}^{L} \mathbf{x}[n],$$
$$\mathbf{C} = [\ \boldsymbol{q}_1(\mathbf{U}\mathbf{U}^T), \boldsymbol{q}_2(\mathbf{U}\mathbf{U}^T), \ldots, \boldsymbol{q}_{N-1}(\mathbf{U}\mathbf{U}^T)\ ]$$

where $\mathbf{U} = [\ \mathbf{x}[1] - \mathbf{d}, \ldots, \mathbf{x}[L] - \mathbf{d}\ ] \in \mathbb{R}^{M \times L}$.

Step 2. Obtain the dimension-reduced pixels $\tilde{\mathbf{x}}[n] = \mathbf{C}^\dagger(\mathbf{x}[n] - \mathbf{d})$ for all n.

Step 3. Set $i := 1$ and $\varrho := |\det(\mathbf{H})|$. Obtain a feasible initial $(\mathbf{H}, \mathbf{g})$ by solving the LP feasibility problem in (43).

Step 4. Solve the LPs

$$\begin{aligned} p^\star = \max_{\mathbf{h}_i^T,\, g_i} \quad & \sum_{j=1}^{N-1} (-1)^{i+j} h_{ij} \det(\boldsymbol{\mathcal{H}}_{ij}) \\ \text{s.t.} \quad & 0 \le \mathbf{h}_i^T \tilde{\mathbf{x}}[n] - g_i \le 1 - \sum_{j \ne i} \mathbf{h}_j^T \tilde{\mathbf{x}}[n] + g_j, \ \forall\, n. \end{aligned}$$

$$\begin{aligned} q^\star = \min_{\mathbf{h}_i^T,\, g_i} \quad & \sum_{j=1}^{N-1} (-1)^{i+j} h_{ij} \det(\boldsymbol{\mathcal{H}}_{ij}) \\ \text{s.t.} \quad & 0 \le \mathbf{h}_i^T \tilde{\mathbf{x}}[n] - g_i \le 1 - \sum_{j \ne i} \mathbf{h}_j^T \tilde{\mathbf{x}}[n] + g_j, \ \forall\, n. \end{aligned}$$

and obtain their optimal solutions, denoted by $(\bar{\mathbf{h}}_i^T, \bar{g}_i)$ and $(\underline{\mathbf{h}}_i^T, \underline{g}_i)$, respectively.

Step 5. If $|p^\star| > |q^\star|$, then update $(\mathbf{h}_i^T, g_i) := (\bar{\mathbf{h}}_i^T, \bar{g}_i)$. Otherwise, update $(\mathbf{h}_i^T, g_i) := (\underline{\mathbf{h}}_i^T, \underline{g}_i)$.

Step 6. If (i modulo $(N-1)$) $\ne 0$, then $i := i + 1$, and go to **Step 4**, else

If $|\max\{|p^\star|, |q^\star|\} - \varrho|/\varrho < \varepsilon$, then $\mathbf{H}^\star = \mathbf{H}$ and $\mathbf{g}^\star = \mathbf{g}$. Otherwise, set $\varrho := \max\{|p^\star|, |q^\star|\}$, $i := 1$, and go to **Step 4**.

Step 7. Calculate $\widehat{\boldsymbol{\alpha}}_N = (\mathbf{H}^\star)^{-1}\mathbf{g}^\star$ and $[\widehat{\boldsymbol{\alpha}}_1, \ldots, \widehat{\boldsymbol{\alpha}}_{N-1}] = \widehat{\boldsymbol{\alpha}}_N \mathbf{1}_{N-1}^T + (\mathbf{H}^\star)^{-1}$.

Step 8. Obtain endmember estimates $\widehat{\mathbf{a}}_i = \mathbf{C}\widehat{\boldsymbol{\alpha}}_i + \mathbf{d}$ for $i = 1, \ldots, N$.

Step 9. Recover the abundance vectors

$$\widehat{\mathbf{s}}[n] = [\ (\mathbf{H}^\star \tilde{\mathbf{x}}[n] - \mathbf{g}^\star)^T \quad 1 - \mathbf{1}_{N-1}^T (\mathbf{H}^\star \tilde{\mathbf{x}}[n] - \mathbf{g}^\star)\ ]^T$$

for $n = 1, \ldots, L$.

V. COMPUTER SIMULATIONS

To demonstrate the efficacy of the proposed MVES algorithm, four Monte Carlo simulations are presented in this section. Each Monte Carlo simulation is based on 100 randomly generated realizations. Section V-A presents some results for data with different purity levels for the noiseless case. Section V-B presents the results for different number of endmembers. Sections V-C and D consider white and nonuniform noise scenarios for different SNRs, respectively. We also tested seven existing algorithms, N-FINDR [15], PPI [14], VCA [17], APS [20], MVC-NMF [26], MVSA [30], and ICE [21] for performance comparison. Note that the first three algorithms require the pure pixel assumption, while the other four do not.

The simulation settings for each unmixing algorithm under test are as follows. In PPI, the number of skewers (which is data dependent) was set to 1000 beyond which no further performance improvements were noticeable in the simulations. The affine set fitting [29] (as presented in Section III) was used for dimension reduction in N-FINDR, PPI, and MVES algorithm. Since PPI, N-FINDR, and VCA are endmember extraction algorithms only, the FCLS [19] was used to find their associated abundances. To distinguish such abundance extraction estimates, we term them as N-FINDR-FCLS, PPI-FCLS, and VCA-FCLS, respectively. Since the operations of APS, MVC-NMF, and ICE are data dependent, the regularization parameters in APS, MVC-NMF, and ICE were set to the values between 0.01 and 0.0001 to ensure the best performance. The convergence accuracy for APS, MVC-NMF, and ICE was set to 10^{-6}, and the convergence tolerance in MVES algorithm was set to $\varepsilon = 10^{-7}$. We should mention that APS, MVC-NMF, ICE, and MVSA were initialized by the endmember and abundance estimates of VCA-FCLS.

Let $\hat{\mathbf{a}}_1, \ldots, \hat{\mathbf{a}}_N$ denote a set of the endmembers estimates, and let $\boldsymbol{s}_1, \ldots, \boldsymbol{s}_N$ and $\hat{\boldsymbol{s}}_1, \ldots, \hat{\boldsymbol{s}}_N$ denote the true and estimated abundances, respectively, where $\boldsymbol{s}_i = [s_i[1], \ldots, s_i[L]]^T \in \mathbb{R}^L$ and $\hat{\boldsymbol{s}}_i = [\hat{s}_i[1], \ldots, \hat{s}_i[L]]^T \in \mathbb{R}^L$. The root-mean-square (rms) spectral angle distance between endmembers and their estimates was used as a performance measure [17]:

$$\phi_{en} = \min_{\boldsymbol{\pi} \in \Pi_N} \sqrt{\frac{1}{N}\sum_{i=1}^{N}\left[\arccos\left(\frac{\mathbf{a}_i^T \hat{\mathbf{a}}_{\pi_i}}{\|\mathbf{a}_i\|\|\hat{\mathbf{a}}_{\pi_i}\|}\right)\right]^2} \tag{44}$$

where $\boldsymbol{\pi} = (\pi_1, \ldots, \pi_N)$, and $\Pi_N = \{\boldsymbol{\pi} \in \mathbb{R}^N \mid \pi_i \in \{1, 2, \ldots, N\},\ \pi_i \ne \pi_j \text{ for } i \ne j\}$ is the set of all the permuta-

Authorized licensed use limited to: Chinese University of Hong Kong. Downloaded on October 21, 2009 at 21:45 from IEEE Xplore. Restrictions apply.

tions of $\{1, 2, \ldots, N\}$. Similarly, the performance measure for the estimated abundances was

$$\phi_{ab} = \min_{\boldsymbol{\pi} \in \Pi_N} \sqrt{\frac{1}{N} \sum_{i=1}^{N} \left[\arccos \left(\frac{\boldsymbol{s}_i^T \hat{\boldsymbol{s}}_{\pi_i}}{\|\boldsymbol{s}_i\| \|\hat{\boldsymbol{s}}_{\pi_i}\|} \right) \right]^2}. \quad (45)$$

It is clear that the smaller the values of ϕ_{en} and ϕ_{ab}, the better the performance of the unmixing algorithm. The performance measures defined in (44) and (45) themselves are optimal assignment problems due to $N!$ permutations $\boldsymbol{\pi}$, but it can be efficiently solved by Hungarian algorithm[1] [41].

As for the computational complexity comparison of the proposed MVES algorithm and the other seven unmixing methods, the computation time (in secs) of each algorithm (implemented in Mathworks Matlab 7.0) running in a desktop computer (equipped with Pentium 4 CPU 3.03 GHz, 4 GB memory) was used as our computational complexity measure.

A. Monte Carlo Simulations For Data With Various Purity Levels

Six endmembers (i.e., Alunite, Buddingtonite, Calcite, Copiapite, Kaolinite, and Muscovite) with 417 bands selected from the U.S. geological survey (USGS) library [42] [see Fig. 4] were used to produce 1000 observed pixels (i.e., $N = 6$, $M = 417$, $L = 1000$). The corresponding abundances were generated following a Dirichlet distribution with $\boldsymbol{\mu} = (\mu_1, \ldots, \mu_N)^T = (1/N)\mathbf{1}_N$ [17], given by

$$D(\mathbf{s}, \boldsymbol{\mu}) = \frac{\prod_{i=1}^{N} \Gamma(\mu_i)}{\Gamma(\sum_{i=1}^{N} \mu_i)} \prod_{i=1}^{N} s_i^{\mu_i - 1} \quad (46)$$

where $\mathbf{s} = (s_1, \ldots, s_N)^T$, $0 \leq s_i \leq 1$, $\sum_{i=1}^{N} s_i = 1$, and $\Gamma(\cdot)$ denotes the Gamma function. Note that the expected value of the ith fraction s_i is $E[s_i] = \mu_i / \sum_{i=1}^{N} \mu_i$. The Dirichlet distribution of the abundances automatically enforces A1) and A2).

To generate the observed data set with different purity levels, let us define a purity measure for an observed pixel $\mathbf{x}[n]$, indicating how quantitatively $\mathbf{x}[n] = \mathbf{A}\mathbf{s}[n]$ is dominated by a single endmember, as follows:

$$\rho_n = \frac{\|\mathbf{s}[n]\|}{\mathbf{1}_N^T \mathbf{s}[n]} = \|\mathbf{s}[n]\| \quad (47)$$

due to A2). Note that $1/\sqrt{N} \leq \rho_n \leq 1$ and the purity of the observed pixel $\mathbf{x}[n]$ is higher for larger ρ_n. A set of L observed pixels $\mathbf{x}[n]$ with $\rho - 0.1 \leq \rho_n \leq \rho$ is called a data set with purity level of ρ (where $(0.1 + 1/\sqrt{N}) \leq \rho \leq 1$), which can be generated through the following steps.

S1) Generate a set of $K = 10L$ observed pixels where the abundance vectors $\mathbf{s}[k]$ following a Dirichlet distribution, i.e.,

$$\Omega = \left\{ \mathbf{x}[k] = \mathbf{A}\mathbf{s}[k] \middle| \mathbf{s}[k] \sim D(\mathbf{s}[k], \boldsymbol{\mu}), \forall\, k = 1, \ldots, K \right\}$$

and calculate the corresponding purity $\rho_k = \|\mathbf{s}[k]\|$ of each $\mathbf{x}[k]$ for all k.

S2) Construct a set of observed pixels with purity level equal to ρ by randomly picking L observed pixels from Ω while satisfying $\rho_n \in [\rho - 0.1, \rho]$, i.e.,

$$\{\mathbf{x}[n] | \mathbf{x}[n] \in \Omega, \rho_n \in [\rho - 0.1, \rho], \forall\, n = 1, \ldots, L\}.$$

Note that the generated data for $\rho = 1$ include some $\mathbf{x}[n]$ with $\rho_n \simeq 1$, i.e., highly pure pixels.

The average ϕ_{en} and ϕ_{ab} of the unmixing methods under test for different values of $\rho = 0.7, 0.75, \ldots, 1$ are shown in Figs. 5 and 6, respectively. One can see from Figs. 5 and 6 that all the algorithms perform better for higher purity level. Obviously, all the algorithms achieve almost perfect unmixing (i.e., $\phi_{en} = \phi_{ab} = 0$) for $\rho = 1$. The ICE, MVC-NMF, MVSA, and MVES algorithm provide better robustness against lower ρ, while the performance of N-FINDR-FCLS, PPI-FCLS, VCA-FCLS, and APS degrades significantly. In addition, the MVSA and proposed MVES algorithm outperform all the other algorithms. The results also validate the endmember identifiability of the MVES belief for $\rho = 1$ (see Theorem 1), and support our conjecture that the MVES belief can also achieve accurate endmember identification when $\rho < 1$.

The average computation time (secs) per realization of each unmixing method for the noiseless case is shown in Table II. From this table, one can observe that the average computation time spent by the pure-pixel based unmixing algorithms, N-FINDR-FCLS, PPI-FCLS, and VCA-FCLS, are less than that of the other algorithms that do not require pure pixels. Among the algorithms without need of pure pixels, the proposed MVES algorithm spent less computation time than MVC-NMF and ICE, but more than APS and MVSA.

The complexity results in Table II also indicate that the proposed MVES algorithm has relatively high complexity (though not the highest). As a future direction, the complexity of MVES may be reduced by making specialized LP algorithms, and by introducing a warm start for each LP in running the MVES algorithm.

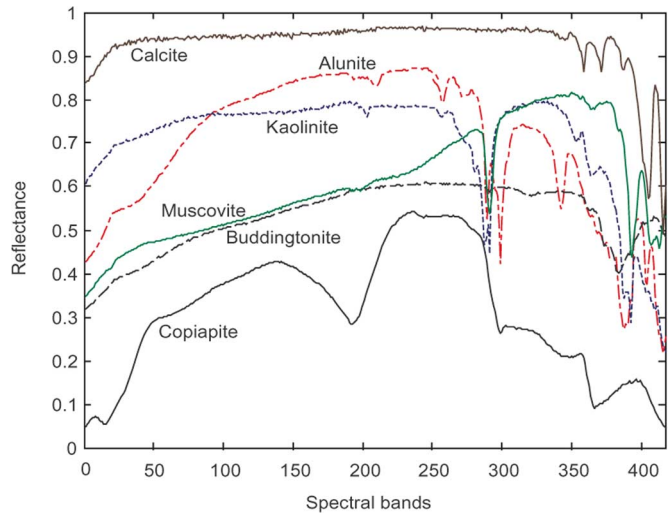

Fig. 4. USGS library spectra of the six minerals: Alunite, Buddingtonite, Calcite, Copiapite, Kaolinite, and Muscovite.

[1]A Matlab implementation is available at http://si.utia.cas.cz/Tichavsky.html.

Authorized licensed use limited to: Chinese University of Hong Kong. Downloaded on October 21, 2009 at 21:45 from IEEE Xplore. Restrictions apply.

TABLE II
THE AVERAGE COMPUTATION TIME (SECS) PER REALIZATION OF THE VARIOUS UNMIXING METHODS IN TWO SCENARIOS

Scenarios	N-FINDR-FCLS	PPI-FCLS	VCA-FCLS	APS	MVC-NMF	MVSA	ICE	MVES
No noise (Sec. V-A)	3.35	3.23	3.06	40.70	64.54	4.08	81.37	54.79
With noise (Sec. V-C)	3.37	3.42	5.62	31.55	54.57	17.11	96.95	47.34

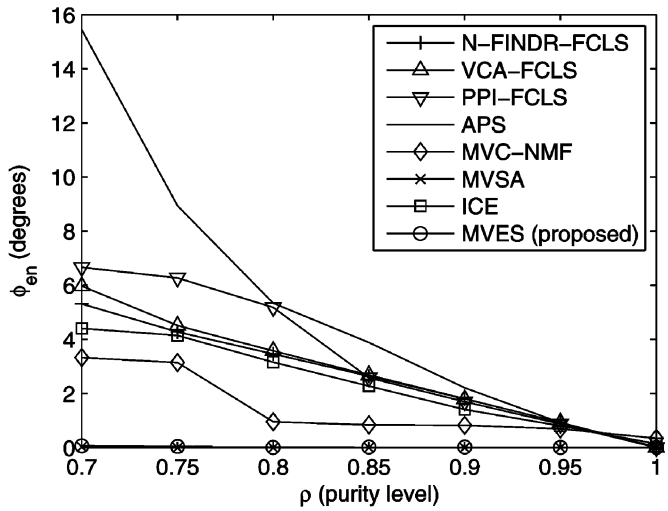

Fig. 5. Simulation results of different purity levels (ϕ_{en}) for the endmember estimates obtained by the various algorithms.

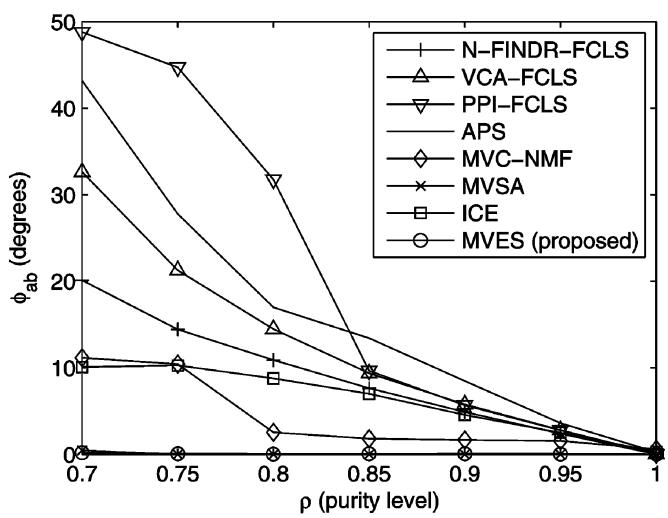

Fig. 6. Simulation results of different purity levels (ϕ_{ab}) for the abundance estimates obtained by the various algorithms.

B. Monte Carlo Simulations for Various Number of Endmembers

The synthetic data were generated in the same manner as in Section V-A, where the purity level was given by $\rho = 0.75$ and the N endmembers were randomly picked from USGS library [42].

The average ϕ_{en} and ϕ_{ab} of the unmixing methods for $N = 6, 8, \ldots, 14$ are shown in Figs. 7 and 8, respectively. One can observe that the performance of the unmixing algorithms (except MVSA and MVES algorithm) slightly degrade as the number of endmembers increases. Specifically, MVSA and our MVES

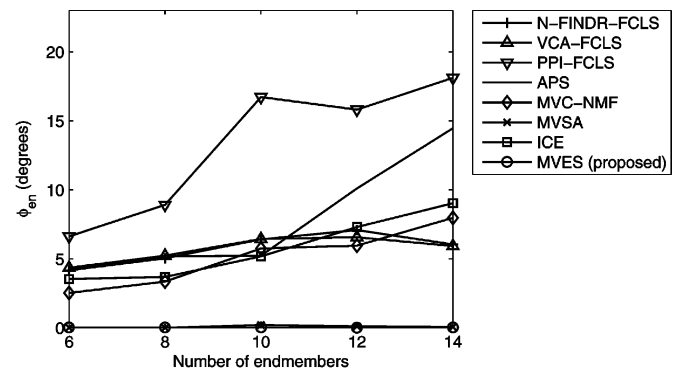

Fig. 7. Simulation results of different number of endmembers (ϕ_{en}) for the endmember estimates obtained by the various algorithms.

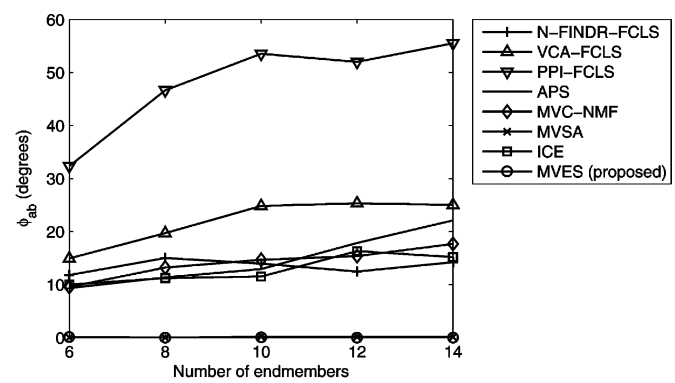

Fig. 8. Simulation results of different number of endmembers (ϕ_{ab}) for the abundance estimates obtained by the various algorithms.

algorithm show the best performance, and the PPI-FCLS is the worst one, among the algorithms under test.

C. Monte Carlo Simulations for Various SNRs

The noise-free synthetic data $\mathbf{x}[n]$ were generated in the same manner as in Section V-A. The noisy data were obtained by adding independent and identically distributed (i.i.d.) zero-mean Gaussian noise to the noise-free data for different values of SNR, where

$$\mathrm{SNR} = \frac{\sum_{n=1}^{L} \|\mathbf{x}[n]\|^2}{\sigma^2 ML}$$

in which σ^2 is the noise variance. To maintain nonnegativity of the noisy observed pixels, we artificially set the negative values of the noisy pixels to zero. Again 100 Monte Carlo runs were performed to evaluate the performance of the unmixing algorithms under test.

Authorized licensed use limited to: Chinese University of Hong Kong. Downloaded on October 21, 2009 at 21:45 from IEEE Xplore. Restrictions apply.

TABLE III
PERFORMANCE COMPARISON OF AVERAGE ϕ_{en} AND ϕ_{ab} (DEGREES) OVER THE VARIOUS UNMIXING METHODS FOR DIFFERENT PURITY LEVELS (ρ) AND SNRS

Methods	ρ	ϕ_{en} SNR (dB)						ϕ_{ab} SNR (dB)					
		20	25	30	35	40	∞	20	25	30	35	40	∞
PPI-FCLS	0.7	6.24	6.09	6.02	6.05	6.01	6.66	44.77	45.80	46.27	46.60	45.78	48.78
	0.85	4.05	3.56	2.77	2.78	2.71	2.58	23.46	20.02	12.02	11.59	10.82	9.65
	1	1.46	**0.58**	0.33	**0.17**	**0.09**	**0**	7.59	3.46	**2.04**	**1.21**	**0.70**	0.02
N-FINDR-FCLS	0.7	5.45	5.31	5.24	5.11	5.16	5.30	22.54	21.86	21.63	19.76	19.82	20.10
	0.85	2.65	2.67	2.66	2.65	2.61	2.63	9.60	8.37	8.03	7.93	7.77	7.64
	1	1.15	0.58	0.33	0.18	0.10	**0**	6.14	3.59	2.13	1.24	0.72	0.02
VCA-FCLS	0.7	5.77	5.56	5.64	5.56	5.50	5.96	31.57	29.97	29.71	28.54	28.38	32.62
	0.85	2.79	2.70	2.67	2.71	2.61	2.68	10.83	9.45	9.00	8.89	8.82	9.37
	1	**1.12**	0.61	**0.32**	0.18	0.11	**0**	**6.00**	**3.45**	2.05	1.23	0.76	0.03
APS	0.7	8.22	7.56	7.79	7.22	6.98	15.44	28.45	28.13	27.49	24.98	26.83	43.16
	0.85	4.16	4.27	4.04	3.93	4.01	3.88	18.56	15.67	13.98	13.67	13.11	13.43
	1	2.75	1.55	1.25	1.10	1.01	0.02	12.59	7.18	4.99	4.75	4.47	0.23
MVC-NMF	0.7	6.80	5.32	4.50	6.05	4.49	3.32	26.69	20.55	16.54	21.89	15.60	11.16
	0.85	**2.47**	**1.37**	**1.31**	**1.34**	1.32	0.84	**5.81**	**4.61**	**4.26**	4.27	4.18	1.81
	1	1.48	0.89	0.71	0.66	0.64	0.35	7.87	4.52	2.87	2.07	1.75	0.59
MVSA	0.7	5.95	4.03	2.67	2.12	1.40	**0.03**	20.80	14.56	7.88	4.81	3.14	0.45
	0.85	5.99	3.75	2.61	2.07	1.27	**0**	19.65	12.12	7.17	**4.16**	**2.34**	**0**
	1	6.12	3.96	2.71	2.14	1.33	**0**	18.93	11.55	6.68	3.85	2.15	**0**
ICE	0.7	6.43	5.13	4.21	4.22	4.22	4.41	24.13	17.85	12.03	12.23	12.62	10.09
	0.85	2.86	2.76	2.79	2.78	2.79	2.27	9.45	8.66	8.58	8.40	8.48	6.99
	1	1.69	1.50	1.47	1.42	1.36	0.14	7.21	6.63	6.28	5.64	4.88	0.26
MVES	0.7	**5.17**	**3.26**	**2.43**	**1.73**	**1.01**	0.06	**16.66**	**10.58**	**6.51**	**3.81**	**2.17**	**0.17**
	0.85	5.28	3.59	2.65	1.85	**1.11**	0.02	16.88	10.98	7.20	4.26	2.38	0.08
	1	6.67	4.37	3.35	2.50	1.55	**0**	19.81	13.09	9.58	6.81	4.50	0.02

The average ϕ_{en} and ϕ_{ab} of all the unmixing algorithms over $\mathrm{SNR} = 15, 20, \ldots, 40, \infty$ dB and $\rho = 0.7, 0.85, 1$ are shown in Table III, where each bold-faced number denotes the minimum rms spectral angle associated with a specific pair of (ρ, SNR) over all the algorithms. Some observations from Table III are as follows. Basically, for a fixed SNR most algorithms (except for MVSA and the proposed MVES) perform better for higher purity level. For a fixed purity level, most algorithms (without involving pure pixels, i.e., MVC-NMF, MVSA, ICE, and MVES) perform better for higher SNR. This is also true for APS and PPI-FCLS for $\rho = 0.85$ and $\rho = 1$, and true for N-FINDR-FCLS and VCA-FCLS for $\rho = 1$. Specifically, in terms of ϕ_{en}, the proposed MVES algorithm performs best for $\rho = 0.7$ and $20 \leq \mathrm{SNR} \leq 40$ dB, and $\rho = 0.85$ and $\mathrm{SNR} = 40\ dB$, and in terms of ϕ_{ab}, the MVES algorithm outperforms all the other algorithms for $\rho = 0.7$ and any SNR. The pure-pixel based methods, PPI-FCLS, N-FINDR-FCLS, and VCA-FCLS generally perform better than the other algorithms for $\rho = 1$ and $\mathrm{SNR} \leq 40$ dB. However, the proposed MVES algorithm shows slightly worse performance as purity level increases, so does MVSA. The reason for this may be due to their slight susceptibility to noise effects. Nevertheless, their performances for $\mathrm{SNR} = \infty$ indeed become better as purity level increases. On the other hand, the average computation time (secs) per realization for each unmixing method for the noisy case is also displayed in Table II. The complexity comparison results of all the algorithms are similar to those in the noise-free case.

D. Monte Carlo Simulations for Nonuniform Noise

Here we consider a more realistic scenario where noise variances over spectral bands are nonuniform. To do this, we generated independent zero-mean Gaussian noise for the M spectral bands, whose variances denoted as $\sigma_1^2, \ldots, \sigma_M^2$ follow a Gaussian shape centered at the $(M/2)$th band [13], i.e.,

$$\sigma_i^2 = \sigma^2 \frac{e^{-((i-M/2)^2/2\eta^2)}}{\sum_{j=1}^{M} e^{-((j-M/2)^2/2\eta^2)}}, \quad \forall\, i = 1, \ldots, M \tag{48}$$

where η controls the variance of the Gaussian shape among $\sigma_1^2, \ldots, \sigma_M^2$. It corresponds to white noise for $\eta = \infty$, and one-band noise for $\eta = 0$.

The average ϕ_{en} and ϕ_{ab} of all the unmixing algorithms for $\rho = 0.75$, $\mathrm{SNR} = 20, 25, \ldots, 40$ dB, $\eta = \infty, 18, 9$ are shown in Table IV, where each bold-faced number again is the minimum rms spectral angle associated with a specific pair of (η, SNR) over all the algorithms. One can see that while the performance of our MVES algorithm almost outperforms all the other algorithms under the white noise scenario $(\eta = \infty)$, MVES algorithm may lose its leading performance for some nonuniform noise scenarios $(\eta = 18, 9)$. Nevertheless, MVES shows competitive performance in general. Our speculation is that the affine set fitting in MVES may not provide very accurate affine subspace estimates (i.e., $\mathbf{d}$ and $\mathbf{C}$ in (6) and (7), respectively) in the presence of nonuniform noise. To mitigate this problem, a recently proposed subspace identification method [13] that considers the nonuniform noise may provide more accurate subspace estimates than those used in this paper. This may be an interesting future direction to pursue.

The above Monte Carlo simulation results (as shown in Figs. 5–8, and Tables III and IV) demonstrate the efficacy of the proposed MVES algorithm, and show that the MVES algorithm performs better than N-FINDR-FCLS, VCA-FCLS, PPI-FCLS, APS, MVC-NMF, and ICE for both the noiseless and noisy cases (especially for data with lower purity levels). Regarding the comparison of MVSA and our MVES algorithm,

Authorized licensed use limited to: Chinese University of Hong Kong. Downloaded on October 21, 2009 at 21:45 from IEEE Xplore. Restrictions apply.

TABLE IV
PERFORMANCE COMPARISON OF AVERAGE ϕ_{en} AND ϕ_{ab} (DEGREES) OVER THE VARIOUS UNMIXING METHODS FOR WHITE NOISE ($\eta = \infty$) AND NON-UNIFORM NOISE ($\eta = 18, 9$), AND PURITY LEVEL $\rho = 0.75$

Methods	η	ϕ_{en} SNR (dB)					ϕ_{ab} SNR (dB)				
		20	25	30	35	40	20	25	30	35	40
PPI-FCLS	∞	6.48	6.74	6.09	6.07	6.11	44.60	49.68	45.18	47.65	40.66
	18	7.08	6.43	6.39	6.29	6.01	47.04	48.29	48.68	41.26	42.13
	9	8.75	6.61	6.32	6.21	6.29	55.63	48.04	42.97	44.67	44.90
N-FINDR-FCLS	∞	**4.51**	4.57	4.48	4.38	4.51	15.75	14.84	14.31	14.11	14.12
	18	4.77	4.48	4.30	4.50	4.49	17.69	14.71	14.08	14.33	13.98
	9	6.06	4.58	4.22	4.54	4.36	34.32	15.83	14.90	15.53	14.97
VCA-FCLS	∞	5.76	5.40	5.39	5.00	4.86	27.59	28.63	26.08	25.94	23.94
	18	5.86	5.19	5.13	5.10	4.93	33.81	28.02	27.31	25.24	23.60
	9	**6.01**	5.74	4.56	4.91	4.94	38.78	33.31	24.18	22.87	25.5
APS	∞	4.36	4.98	4.61	4.37	4.12	17.53	17.18	15.43	15.40	14.89
	18	**5.03**	4.79	4.28	4.29	4.32	22.61	18.57	16.50	15.74	14.42
	9	7.54	6.31	3.93	4.38	3.23	32.41	22.54	17.31	14.61	13.75
MVC-NMF	∞	5.42	4.21	2.95	2.71	1.70	**16.22**	16.68	15.51	9.42	7.14
	18	5.14	3.37	2.66	2.60	2.21	26.20	12.29	8.13	8.17	8.32
	9	6.60	7.00	3.60	2.08	2.60	29.60	28.79	14.91	8.25	8.47
MVSA	∞	5.28	3.75	2.77	2.11	1.17	19.48	12.75	7.49	4.41	2.52
	18	9.21	4.09	**2.26**	**1.31**	**0.71**	27.95	12.93	**5.85**	**3.18**	**1.73**
	9	10.13	9.15	2.43	**1.35**	**0.62**	37.78	31.85	**4.12**	**3.25**	**1.67**
ICE	∞	5.83	5.74	5.65	5.69	5.30	28.36	25.39	25.92	25.07	26.19
	18	5.40	5.37	5.37	4.64	5.30	25.47	25.49	24.21	30.75	26.19
	9	5.40	5.29	5.40	5.16	5.46	**26.11**	27.59	26.47	25.16	27.41
MVES	∞	5.18	**3.30**	**2.47**	**1.74**	**1.05**	16.83	**10.74**	**6.88**	**3.96**	**2.25**
	18	7.11	**3.48**	2.57	1.62	1.16	**22.14**	**10.57**	6.41	4.22	2.36
	9	8.56	**3.67**	**2.09**	1.40	0.73	32.20	**12.23**	5.28	3.65	2.05

we conclude that their performances are very comparable, and in most white noise cases with lower purity levels and various SNRs the MVES algorithm slightly outperforms the MVSA. However, we also see from Table II that MVES algorithm spent more computation time than MVSA. There appears to be a tradeoff between performance and complexity for each algorithm.

VI. REAL HYPERSPECTRAL IMAGE EXPERIMENTS

We applied the VCA-FCLS [17], [19], MVC-NMF [26], and the proposed MVES algorithm to process real hyperspectral image data [43], which were collected by airborne visible/infrared imaging spectrometer (AVIRIS) flight over the Cuprite mining site, Nevada, in 1997. This data set has been widely used for remote sensing experiments [4], [17], [26], and it consists of 224 spectral channels with 10 nm spectral resolution covering wavelengths ranging from 0.4 to 2.5 μm. The spectral bands 1–2, 104–113, 148–167, and 221–224 were removed due to low SNR and water-vapor absorption. Hence, a total of 188 bands were tested in this experiment. The subimage of the 150th band, including 200 vertical lines with 200 pixels per line is shown in Fig. 9.

One of VD methods [12], the noise-whitened HFC (NWHFC)-based eigenthresholding method with false-alarm probability $P_F = 10^{-5}$, was applied to the data set to estimate the number of endmembers, and the estimated number of endmembers is $N = 14$. By visually comparing the abundance maps estimated by the MVES algorithm with the ground truth reported in [44], [45], the abundance maps obtained by MVES algorithm are identified as mineral maps of Muscovite, Goethite, Halloysite, Nontronite, Montmorillonite, Alunite, Buddingtonite, Pyrope, Kaolinite #1, Kaolinite #2, Chalcedony, Desert Varnish, Kaolinite #3, and Andradite as shown in Fig. 10(a)–(n), respectively. Likewise, the abundance maps obtained by MVC-NMF are identified as mineral maps

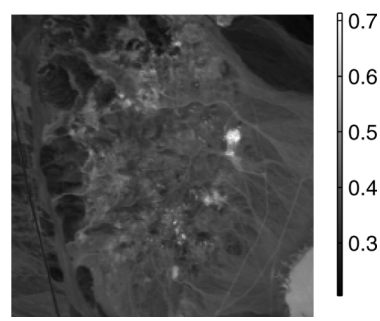

Fig. 9. The subimage of the AVIRIS hyperspectral image data for the 150th band.

of Muscovite, Nontronite, Montmorillonite, Alunite, Buddingtonite, Pyrope, Kaolinite #1, Chalcedony, Desert Varnish, Andradite, Kaolinite #4, and Dumortierite, and those obtained by VCA-FCLS are identified as mineral maps of Muscovite, Nontronite, Montmorillonite, Alunite, Buddingtonite, Pyrope, Kaolinite #1, Chalcedony, Desert Varnish, Andradite, Kaolinite #4, and Dumortierite. The individual abundance maps estimated by MVC-NMF and VCA are omitted here due to space limit, but can be found at http://www.ee.nthu.edu.tw/cychi/HI_results. Furthermore, the endmember estimates obtained by the three unmixing algorithms associated with the identified minerals are also shown in Fig. 11. Fig. 11(a) shows the library spectra of all the identified minerals. The endmember estimates obtained by MVES algorithm are shown in Fig. 11(b), and those obtained by MVC-NMF and VCA are shown in Fig. 11(c) and (d), respectively. One can see from Fig. 11 that fourteen distinct minerals are retrieved by MVES algorithm, while twelve distinct minerals are retrieved by both MVC-NMF and VCA. Although MVC-NMF adds Craig's criterion (as a regularization term) in its objective function, the reason for fewer minerals retrieved by MVC-NMF may be due to its initialization by VCA. By the

Authorized licensed use limited to: Chinese University of Hong Kong. Downloaded on October 21, 2009 at 21:45 from IEEE Xplore. Restrictions apply.

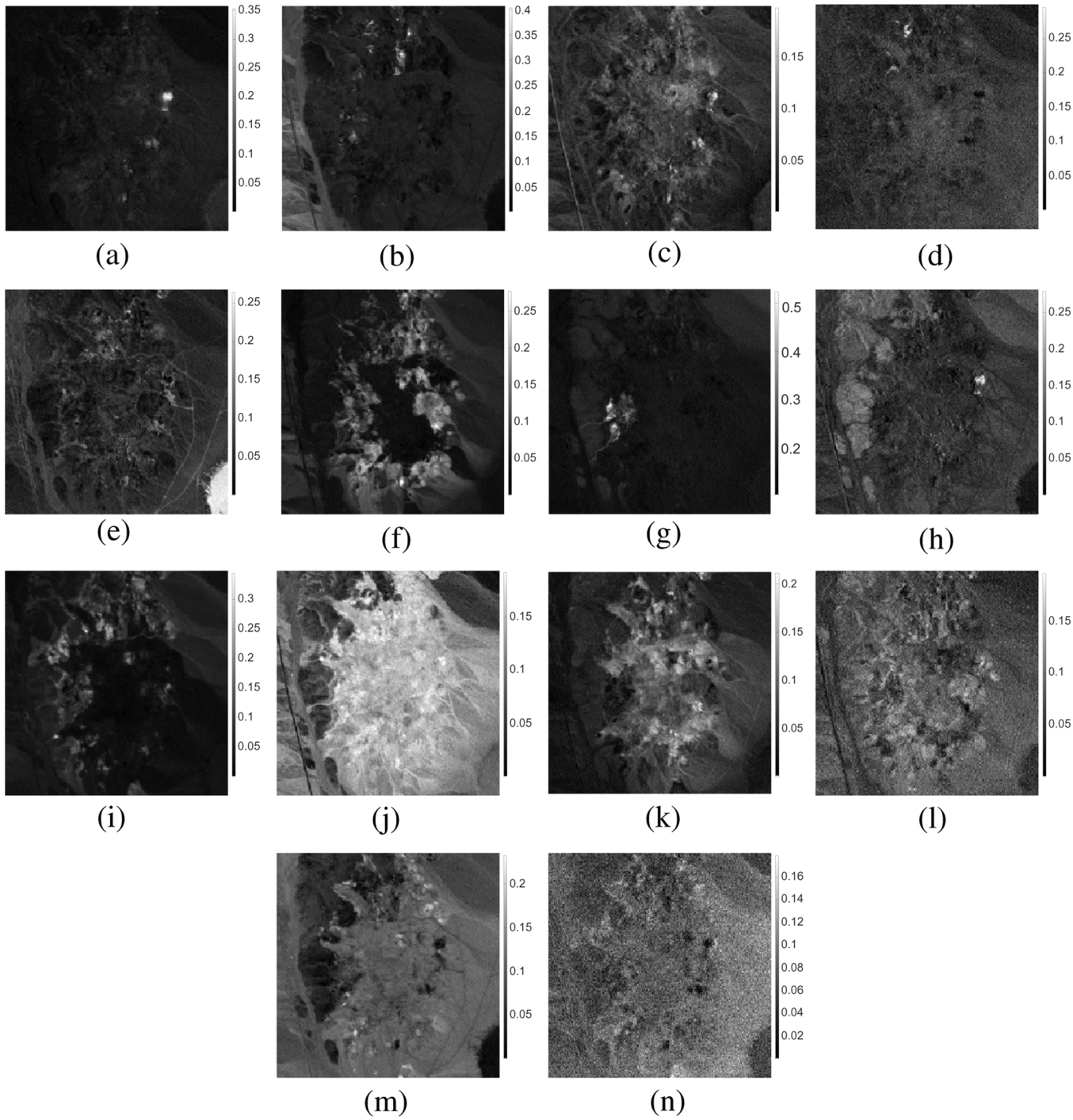

Fig. 10. Fourteen respective estimated abundances obtained by MVES algorithm: (a) Muscovite; (b) Goethite; (c) Halloysite; (d) Nontronite; (e) Montmorillonite; (f) Alunite; (g) Buddingtonite; (h) Pyrope; (i) Kaolinite #1; (j) Kaolinite #2; (k) Chalcedony; (l) Desert Varnish; (m) Kaolinite #3; and (n) Andradite.

same token, one can also observe that MVC-NMF and VCA retrieve the same minerals in this experiment.

To further evaluate the accuracy of the mineral-identified endmember estimates obtained by the three unmixing algorithms, we used the mean-removed spectral angle between each mineral-identified endmember estimate $\widehat{\mathbf{a}}$ and the library spectrum of the identified mineral $\mathbf{a}$ [46] as a performance index, i.e.

$$\phi = \arccos\left(\frac{(\widehat{\mathbf{a}} - \mathbf{m}(\widehat{\mathbf{a}}))^T(\mathbf{a} - \mathbf{m}(\mathbf{a}))}{\|\widehat{\mathbf{a}} - \mathbf{m}(\widehat{\mathbf{a}})\|\|\mathbf{a} - \mathbf{m}(\mathbf{a})\|}\right) \tag{49}$$

where $\mathbf{m}(\mathbf{a}) = \left(\mathbf{1}_M^T\mathbf{a}/M\right)\mathbf{1}_M$ for any vector $\mathbf{a} \in \mathbb{R}^M$.

The values of ϕ associated with the endmember estimates obtained by the three unmixing algorithms are shown in Table V where those numbers in the parentheses stand for the mean-removed spectral angles of the endmember estimates classified as the same mineral. One can see from Table V that the average mean-removed spectral angle associated with MVES algorithm is smaller than that associated with MVC-NMF, but larger than that associated with VCA. The possible cause may be due to serious effect of nonuniform noise on our proposed MVES algorithm, leading to some performance degradation. We would

Authorized licensed use limited to: Chinese University of Hong Kong. Downloaded on October 21, 2009 at 21:45 from IEEE Xplore. Restrictions apply.

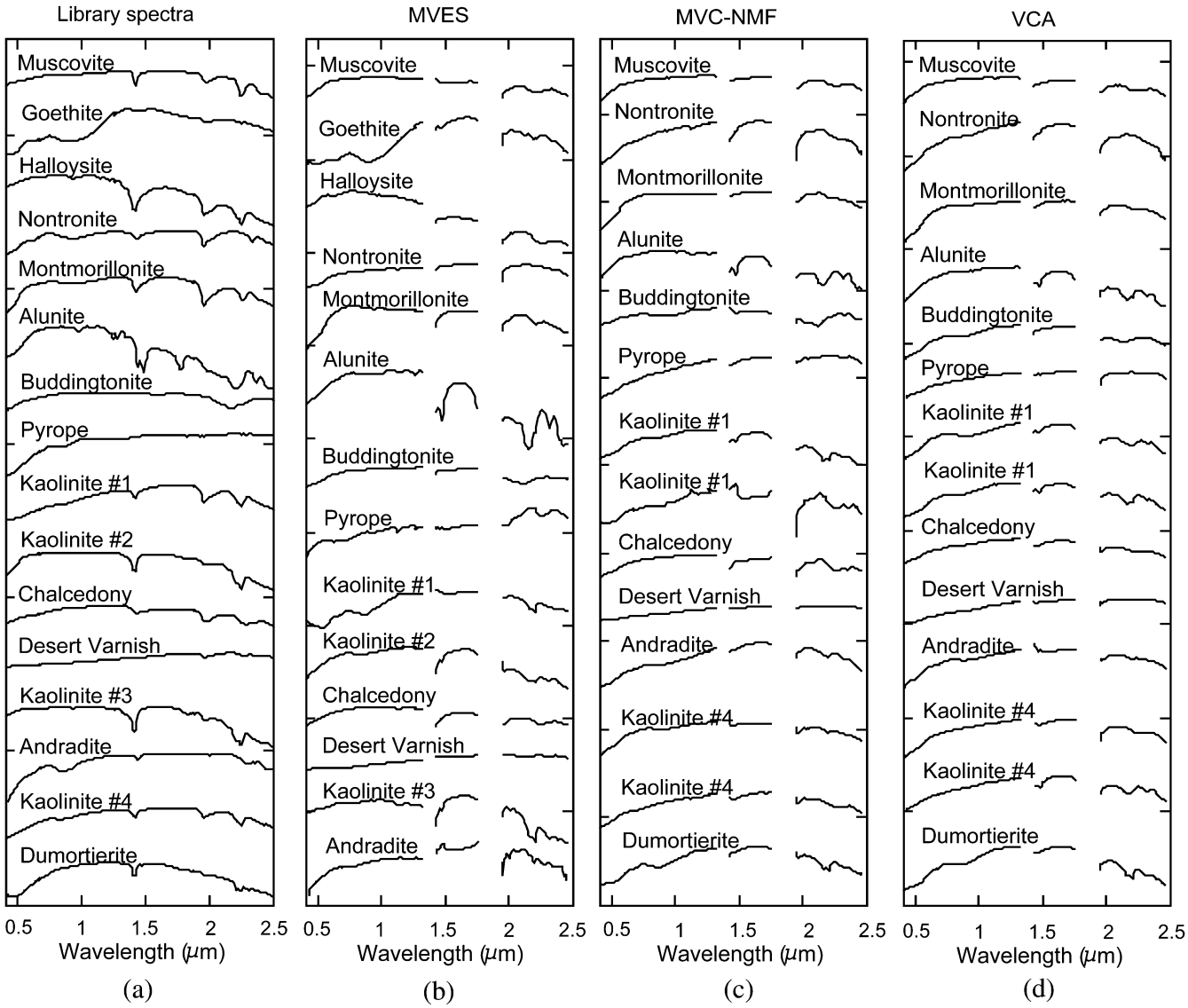

Fig. 11. (a) The endmember signatures provided by the USGS library, and the endmember estimates obtained by: (b) MVES algorithm; (c) MVC-NMF; and (d) VCA.

consider how to deal with the nonuniform noise issues for the MVES algorithm as our future research. Even so, MVES algorithm shows the capability of retrieving some less prevalent minerals, i.e., Goethite and Halloysite, which are not retrieved by MVC-NMF and VCA. Moreover, we also compared the above experimental results to the results reported in [17], [20], [26], [44], [45], and found that they all exhibit a high agreement between them.

VII. Conclusion

We have presented a convex analysis based MVES algorithm for hyperspectral unmixing without involving pure pixels. Through an affine set fitting of observed pixels followed by the use of Craig's unmixing criterion, the MVES problem was cast as a problem of minimizing a simplex volume subject to the constraint that all the dimension-reduced pixels be enclosed in the simplex. The proposed MVES algorithm utilizes LPs to approximate the MVES problem in a cyclic fashion, and is easy to implement since LP softwares are readily available today.

TABLE V
Mean-Removed Spectral Angles ϕ (Degrees) Between Library Spectra and Endmembers Estimated by MVES Algorithm, MVC-NMF, and VCA

	MVES	MVC-NMF	VCA
Muscovite	35.64	33.93	32.70
Goethite	15.08	-	-
Halloysite	13.10	-	-
Nontronite	29.74	20.21	16.14
Montmorillonite	25.54	19.81	15.98
Alunite	19.55	18.97	23.48
Buddingtonite	20.68	36.91	27.25
Pyrope	32.37	14.49	19.97
Kaolinite #1	22.95	27.74 (31.84)	22.55 (22.04)
Kaolinite #2	21.32	-	-
Chalcedony	26.01	23.02	31.09
Desert Varnish	14.74	15.69	16.13
Kaolinite #3	17.52	-	-
Andradite	26.80	19.21	18.16
Kaolinite #4	-	19.77 (12.00)	18.17 (21.05)
Dumortierite	-	33.34	20.44
Average ϕ	22.92	23.35	21.80

Authorized licensed use limited to: Chinese University of Hong Kong. Downloaded on October 21, 2009 at 21:45 from IEEE Xplore. Restrictions apply.

We also discussed the endmember identifiability of the MVES criterion, and proved it under the existence of pure pixels. Some computer simulation results were presented to demonstrate that the proposed MVES algorithm outperforms some existing benchmark hyperspectral unmixing algorithms, especially for data sets with lower purity levels. Some experimental results with real hyperspectral image data also show that the proposed MVES algorithm can estimate endmembers and abundances both in a high agreement with the reported ground truth.

ACKNOWLEDGMENT

The authors would like to sincerely thank Dr. J. M. Bioucas-Dias for his valuable comments and suggestions to the implementation of MVSA algorithm, and Dr. H. Qi and A. Zymnis who kindly provided us with the pseudocodes of MVC-NMF and APS, respectively.

REFERENCES

[1] T. M. Lillesand, R. W. Kiefer, and J. W. Chipman, *Remote Sensing and Image Interpretation*, 2nd ed. New York: Wiley, 2004.

[2] J. A. Richards, "Analysis of remotely sensed data: The formative decades and the future," *IEEE Trans. Geosci. Remote Sens.*, vol. 43, no. 2, pp. 422–432, Mar. 2005.

[3] B. A. Campbell, *Radar Remote Sensing of Planetary Surfaces*. New York: Cambridge Univ. Press, 2002.

[4] R. N. Clark, G. A. Swayze, K. E. Livo, R. F. Kokaly, S. Sutley, J. B. Dalton, R. R. McDougal, and C. A. Gent, "Imaging spectroscopy: Earth and planetary remote sensing with the USGS tetracorder and expert systems," *J. Geophys. Res.*, vol. 108, no. 12, pp. 5–44, Dec. 2003.

[5] G. Shaw and D. Manolakis, "Signal processing for hyperspectral image exploitation," *IEEE Signal Process. Mag.*, vol. 19, no. 1, pp. 12–16, Jan. 2002.

[6] D. Landgrebe, "Hyperspectral image data analysis," *IEEE Signal Process. Mag.*, vol. 19, no. 1, pp. 17–28, Jan. 2002.

[7] N. Keshava and J. Mustard, "Spectral unmixing," *IEEE Signal Process. Mag.*, vol. 19, no. 1, pp. 44–57, Jan. 2002.

[8] D. Stein, S. Beaven, L. Hoff, E. Winter, A. Schaum, and A. Stocker, "Anomaly detection from hyperspectral imagery," *IEEE Signal Process. Mag.*, vol. 19, no. 1, pp. 58–69, Jan. 2002.

[9] N. Keshava, "A survey of spectral unmixing algorithms," *Lincoln Lab. J.*, vol. 14, no. 1, pp. 55–78, Jan. 2003.

[10] M. O. Smith, P. E. Johnson, and J. B. Adams, "Quantitative determination of mineral types and abundances from reflectance spectra using principal component analysis," *J. Geophys. Res.*, vol. 90, no. 2, pp. C797–C804, Oct. 1985.

[11] A. A. Green, "A transformation for ordering multispectral data in terms of image quality with implications for noise removal," *IEEE Trans. Geosci. Remote Sens.*, vol. 32, no. 1, pp. 65–74, May 1988.

[12] C.-I. Chang and Q. Du, "Estimation of number of spectrally distinct signal sources in hyperspectral imagery," *IEEE Trans. Geosci. Remote Sens.*, vol. 42, no. 3, pp. 608–619, Mar. 2004.

[13] J. M. Bioucas-Dias and J. M. P. Nascimento, "Hyperspectral subspace identification," *IEEE Trans. Geosci. Rem. Sens.*, vol. 46, no. 8, pp. 2435–2445, 2008.

[14] J. W. Boardman, F. A. Kruse, and R. O. Green, "Mapping target signatures via partial unmixing of AVIRIS data," in *Proc. Summ. JPL Airborne Earth Sci. Workshop*, Pasadena, CA, Dec. 9–14, 1995, vol. 1, pp. 23–26.

[15] M. E. Winter, "N-findr: An algorithm for fast autonomous spectral end-member determination in hyperspectral data," in *Proc. SPIE Conf. Imaging Spectrometry*, Pasadena, CA, Oct. 1999, pp. 266–275.

[16] M. E. Winter and U. Imagery, "A proof of the N-FINDR algorithm for the automated detection of endmembers in a hyperspectral image," in *Proc. SPIE Conf. Algorithms and Technol. Multispect., Hyperspect. Data*, Aug. 2004, vol. 5425, pp. 31–41.

[17] J. M. P. Nascimento and J. M. Bioucas-Dias, "Vertex component analysis: A fast algorithm to unmix hyperspectral data," *IEEE Trans. Geosci. Remote Sens.*, vol. 43, no. 4, pp. 898–910, Apr. 2005.

[18] A. Ifarraguerri and C.-I. Chang, "Multispectral and hyperspectral image analysis with convex cones," *IEEE Trans. Geosci. Remote Sens.*, vol. 37, no. 2, pp. 756–770, Mar. 1999.

[19] D. Heinz and C.-I. Chang, "Fully constrained least squares linear mixture analysis for material quantification in hyperspectral imagery," *IEEE Trans. Geosci. Remote Sens.*, vol. 39, no. 3, pp. 529–545, Mar. 2001.

[20] A. Zymnis, S.-J. Kim, J. Skaf, M. Parente, and S. Boyd, "Hyperspectral image unmixing via alternating projected subgradients," in *Proc. 41st Asilomar Conf. Signals, Syst.*, Pacific Grove, CA, Nov. 4–7, 2007.

[21] M. Berman, H. Kiiveri, R. Lagerstrom, A. Ernst, R. Dunne, and J. F. Huntington, "ICE: A statistical approach to identifying endmembers in hyperspectral images," *IEEE Trans. Geosci. Remote Sens.*, vol. 42, no. 10, pp. 2085–2095, Oct. 2004.

[22] D. Lee and H. S. Seung, "Learning the parts of objects by non-negative matrix factorization," *Nature*, vol. 401, pp. 788–791, Oct. 1999.

[23] V. P. Pauca, J. Piper, and R. J. Plemmons, "Nonnegative matrix factorization for spectral data analysis," *Linear Algebra Appl.*, vol. 1, no. 416, pp. 29–47, 2006.

[24] N. Dobigeon, S. Moussaoui, M. Coulon, J.-Y. Tourneret, and A. O. Hero, "Joint Bayesian endmember extraction and linear unmixing for hyperspectral imagery," *IEEE Trans. Signal Process.*, 2009, to be published.

[25] M. D. Craig, "Minimum-volume transforms for remotely sensed data," *IEEE Trans. Geosci. Remote Sens.*, vol. 32, no. 3, pp. 542–552, May 1994.

[26] L. Miao and H. Qi, "Endmember extraction from highly mixed data using minimum volume constrained nonnegative matrix factorization," *IEEE Trans. Geosci. Remote Sens.*, vol. 45, no. 3, pp. 765–777, Mar. 2007.

[27] J. W. Boardman, "Automating spectral unmixing of AVIRIS data using convex geometry concepts," in *Proc. Summ. 4th Annu. JPL Airborne Geosci. Workshop*, Dec. 9–14, 1993, vol. 1, pp. 11–14.

[28] J. W. Boardman, "Geometric mixture analysis of imaging spectrometry data," in *Proc. IEEE Int. Geosci. Remote Sens. Symp.*, Pasadena, CA, Aug. 8–12, 1994, vol. 4, pp. 2369–2371.

[29] T.-H. Chan, W.-K. Ma, C.-Y. Chi, and Y. Wang, "A convex analysis framework for blind separation of non-negative sources," *IEEE Trans. Signal Process.*, vol. 56, pp. 5120–5134, Oct. 2008.

[30] J. Li and J. Bioucas-Dias, "Minimum volume simplex analysis: A fast algorithm to unmix hyperspectral data," in *Proc. IEEE Int. Geosci. Remote Sens. Symp.*, Boston, MA, Aug. 8–12, 2008, vol. 4, pp. 2369–2371.

[31] A. Cichocki and S. Amari, *Adaptive Blind Signal and Image Processing*. New York: Wiley, 2002.

[32] J. M. P. Nascimento and J. M. Bioucas-Dias, "Does independent component analysis play a role in unmixing hyperspectral data?," *IEEE Trans. Geosci. Remote Sens.*, vol. 43, pp. 175–187, Jun. 2005.

[33] J. Wang and C.-I. Chang, "Applications of independent component analysis in endmember extraction and abundance quantification for hyperspectral imagery," *IEEE Trans. Geosci. Remote Sens.*, vol. 44, no. 9, pp. 2601–2616, 2006.

[34] S. Boyd and L. Vandenberghe, *Convex Optimization*. Cambridge, U.K.: Cambridge Univ. Press, 2004.

[35] P. Gritzmann and V. Klee, "On the complexity of some basic problems in computational convexity: I.: Containment problems," *Discrete Math.*, vol. 136, no. 1–3, pp. 129–174, Dec. 1994.

[36] Y. Zhou and S. Suri, "Algorithms for a minimum volume enclosing simplex in three dimensions," *SIAM J. Comput.*, vol. 31, no. 5, pp. 1339–1357, 2002.

[37] G. Strang, *Linear Algebra and Its Applications*, 4th ed. San Diego, CA: Thomson, 2006.

[38] F.-Y. Wang, C.-Y. Chi, T.-H. Chan, and Y. Wang, "Non-negative least-correlated component analysis for separation of dependent sources by volume maximization," *IEEE Trans. Pattern Anal. Mach. Intell.*, 2009, to be published.

[39] I. J. Lustig, R. E. Marsten, and D. F. Shanno, "Interior point methods for linear programming: Computational state of the art," *ORSA J. Comput.*, vol. 6, no. 1, pp. 1–14, 1994.

[40] J. F. Sturm, "Using sedumi 1.02, a MATLAB toolbox for optimization over symmetric cones," *Optimiz. Methods Software*, vol. 11–12, pp. 625–653, 1999.

Authorized licensed use limited to: Chinese University of Hong Kong. Downloaded on October 21, 2009 at 21:45 from IEEE Xplore. Restrictions apply.

[41] H. W. Kuhn, "The Hungarian method for the assignment method," *Naval Res. Logist. Quart.*, vol. 2, pp. 83–97, 1955.
[42] Tech. Rep [Online]. Available: http://speclab.cr.usgs.gov/cuprite.html
[43] AVIRIS Free Standard Data Products [Online]. Available: http://aviris.jpl.nasa.gov/html/aviris.freedata.html
[44] G. Swayze, R. Clark, S. Sutley, and A. Gallagher, "Ground-truthing AVIRIS mineral mapping at Cuprite, Nevada," in *Proc. Summer 4th Annu. JPL Airborne Geosci. Workshop*, 1992, vol. 2, pp. 47–49.
[45] G. Swayze, "The hydrothermal and structural history of the cuprite mining district, southwestern Nevada: An integrated geological and geophysical approach," Ph.D. dissertation, Univ. Colorado, Boulder, 1997.
[46] R. N. Clark, G. A. Swayze, A. Gallagher, T. V. King, and W. M. Calvin, "The U.S. geological survey digital spectral library: Version 1: 0.2 to 3.0 μm," *U.S. Geol. Surv., Open File Rep. 93-592*, 1993.

Tsung-Han Chan (S'08) received the B.S. degree from the Department of Electrical Engineering, Yuan Ze University, Taoyuan, Taiwan, in 2004 and the Ph.D. degree from the Institute of Communications Engineering, National Tsing Hua University (NTHU), Hsinchu, Taiwan, in 2009.

Currently, he is a Postdoctoral Research Fellow with the Institute of Communications Engineering, NTHU. In 2008, he was a visiting Doctoral Graduate Research Assistant with Virginia Polytechnic Institute and State University, Arlington. His research interests are in signal processing, convex optimization, and pattern analysis with a recent emphasis on dynamic medical imaging and remote sensing applications.

Chong-Yung Chi (S'83–M'83–SM'89) received the Ph.D. degree in electrical engineering from the University of Southern California, Los Angeles, in 1983.

From 1983 to 1988, he was with the Jet Propulsion Laboratory, Pasadena, CA. He has been a Professor with the Department of Electrical Engineering since 1989 and the Institute of Communications Engineering (ICE) since 1999 (also the Chairman of ICE for 2002–2005), National Tsing Hua University, Hsinchu, Taiwan. He coauthored a technical book, *Blind Equalization and System Identification* (New York: Springer, 2006), and published more than 150 technical (journal and conference) papers. His current research interests include signal processing for wireless communications, convex analysis and optimization for blind source separation, biomedical imaging, and hyperspectral imaging.

Dr. Chi has been a Technical Program Committee member for many IEEE sponsored and cosponsored workshops, symposiums, and conferences on signal processing and wireless communications, including Co-Organizer and general Co-Chairman of IEEE SPAWC 2001, and Co-Chair of Signal Processing for Communications Symposium, ChinaCOM 2008, and ChinaCOM 2009. He was an Associate Editor of the IEEE TRANSACTIONS ON SIGNAL PROCESSING (5/2001–4/2006), IEEE TRANSACTIONS ON CIRCUITS AND SYSTEMS II (1/2006–12/2007), and a member of Editorial Board of EURASIP *Signal Processing Journal* (6/2005–5/2008), and an editor (7/2003–12/2005) as well as a Guest Editor (2006) of EURASIP *Journal on Applied Signal Processing*. Currently, he is an Associate Editor of the IEEE SIGNAL PROCESSING LETTERS and IEEE TRANSACTIONS ON CIRCUITS AND SYSTEMS I, and a member of the IEEE Signal Processing Committee on Signal Processing Theory and Methods.

Yu-Min Huang received the B.S. degree from the Department of Engineering and System Science in 2006 and M.S. degree from the Institute of Communications Engineering in 2008, National Tsing Hua University, Hsinchu, Taiwan.

She is currently working as a Research and Development Engineer with ZyXEL Communications Corp., Hsinchu. Her research interests include wireless communications and hyperspectral imaging.

Wing-Kin Ma (S'96–M'01) received the B.Eng. (first-class honors) degree in electrical and electronic engineering from the University of Portsmouth, Portsmouth, U.K., in 1995 and the M.Phil. and Ph.D. degrees, both in electronic engineering, from the Chinese University of Hong Kong (CUHK), Hong Kong, in 1997 and 2001, respectively.

He is currently an Assistant Professor with the Department of Electronic Engineering, CUHK. From 2005 to 2007, he was also an Assistant Professor with the Institute of Communications Engineering, National Tsing Hua University, Taiwan, R.O.C., where he holds an adjunct position. Prior to becoming a faculty member, he held various research positions with McMaster University, Canada; CUHK, Hong Kong; and the University of Melbourne, Australia. His research interests are in signal processing and communications, with a recent emphasis on MIMO techniques and convex optimization.

Dr. Ma's Ph.D. dissertation was commended to be "of very high quality and well deserved honorary mentioning" by the Faculty of Engineering, CUHK, in 2001. He currently serves as an Associate Editor of the IEEE TRANSACTIONS ON SIGNAL PROCESSING and as a Guest Editor of the IEEE SIGNAL PROCESSING MAGAZINE Special Issue on "Convex Optimization for Signal Processing."

Authorized licensed use limited to: Chinese University of Hong Kong. Downloaded on October 21, 2009 at 21:45 from IEEE Xplore. Restrictions apply.